



**Organic Geochemistry of the Qahash  
Formation in the Offshore  
Well A1-NC 128, Cyrenaica Basin,  
NE Libya**

**By**

**OMAR ADEL OMAR GENIBER**

**Supervisor**

**Assist. Prof. Osama Shaltami**

**This Thesis was submitted in Partial Fulfillment of the  
Requirements for Master's Degree of Science in Geology,  
Geochemistry**

**University of Benghazi**

**Faculty of Science**

**Dec 2019**

Copyright© 2019. All rights reserved, no part of this thesis may be reproduced in any form, electronic or mechanical, including photocopy, recording scanning, or any information, without the permission in writhing from the author or the Directorate of Graduate Studies and Training university of Benghazi.

حقوق الطبع 2019 محفوظة. لا يسمح اخذ اى معلومة من اى جزء من هذه الرسالة على هيئة نسخة الكترونية او ميكانيكية بطريقة التصوير او التسجيل او المسح من دون الحصول على إذن كتابي من المؤلف أو إدارة الدراسات العليا والتدريب جامعة بنغازي



Department of Earth Science

**Organic Geochemistry of the Qahash Formation in the  
Offshore Well A1-NC 128, Cyrenaica Basin, NE Libya**


By

**OMAR ADEL OMAR GENIBER**

This Thesis was Successfully Defended and Approved on **05.12.2019**

Supervisor

**Assist. Prof. Osama Shaltami**

Signature: ..... 

**Associate. Prof. Saad K. Abdalla Ebaidi** (Internal Examiner)

Signature: ..... 

**Prof. Hamad Mohammed Adres** (External Examiner)

Signature: ..... 



**Director of Graduate Studies and Training**



بِسْمِ اللَّهِ الرَّحْمَنِ الرَّحِيمِ

وَمَا أُوتِيَ مِنَ الْعِلْمِ إِلَّا قَلِيلًا

And mankind have not been given of knowledge except a little."

سورة الإسراء، الآية (85)

صَدَقَ اللَّهُ الْعَظِيمُ

## **DEDICATION**

**First to first thank to Allah**

**Every challenging work needs self-efforts as well as guidance of  
elders especially those who were very close to our heart**

**My humble effort I dedicate my sweet and loving**

### **MY FATHER**

**For earning an honest living for us and for supporting and  
encouraging me to believe in myself**

### **MY MOTHER**

**A strong and gentle soul who taught me to trust in Allah believe  
in hard work and that so much could be done with little**

### **MY BROTHERS AND SISTERS**

**whose affection, love, encouragement and make me able to get  
such success and honor**

### **MY WIFE**

**I could never have done this without your faith, support, and  
constant encouragement. thank you for teaching me to believe in  
myself, in god, and in my dreams**

### **MY FRIENDS**

**Especially Hassan Omar and Akram Elrabhi**

### **FINALLY**

**I would like to big thank to all hard working and respected  
teachers in Earth Science Department especially my friend and  
my teacher Dr. Fares Fathi**

**OMAR GENIBER, 2019**

## **ACKNOWLEDGEMENT**

**I would like to express my sincere gratitude to the University of Benghazi, Faculty of Science, Department of Earth Sciences for letting me fulfill my dream of being a student here**

**I would also like to thank the laboratory of Chemostratigraphy and Organic Geochemistry (LGQM), State University of Rio de Janeiro (UERJ), Brazil. And The AGIP Company for giving me the data and opportunity to write an honors thesis**

**To my committee, I am extremely grateful for your assistance and suggestions throughout my project**

**To all my friends and family for helping me survive all the stress from these years and not letting me give up. most of all. I am fully indebted to Assist. Prof. Osama Shaltami, my advisor and director, for his understanding, wisdom, patience, enthusiasm, and encouragement and for pushing me farther than I thought I could go**

**OMAR GENIBER, 2019**

## List of Contents

---

Title	Page
Copyright © 2019	ii
Examination committee	iii
Quran	iv
Dedication	v
Acknowledgement	vi
List of content	vii
List of Tables	ix
List of Figures	x
Abbreviation	xiii
Abstract	xv
1.1. General	1
1.2. Regional Geology	2
1.2.1. Regional Structural Setting	2
1.2.2. Regional Stratigraphic Setting	2
1.2.2.1. Late cretaceous	2
1.2.2.2. Paleocene	3
1.2.2.3. Eocene	6
1.2.2.4. Oligocene	6
1.2.2.5. Miocene	7
1.2.2.6. Pliocene	8
1.2.2.7. Quaternary	9
1.3. Present Study	10
1.3.1. Qahash Formation	10

1.3.2.	Objectives	11
1.3.3.	Previous Work	12
1.3.4.	Stratigraphy	17
1.3.5.	Methodology	19
1.3.5.1.	sampling	19
1.3.5.2.	Organic Petrography	19
1.3.5.3.	Scanning Electron Microscope (SEM)	19
1.3.5.4.	Rock Eval Pyrolysis	20
1.3.5.5.	Gas Chromatography-Mass Spectrometry (GC-MS)	20
2.1.	Introduction	22
2.2.	Vitrinite Group	23
2.3.	Liptinite Group	28
2.4.	Inertinite Group	31
2.5.	Mineral Matter	35
2.6.	Maceral Indices	36
2.7.	Rank of Coal	37
2.8.	Paleovegetation, Paleoclimate and Depositional Environment	39
3.1.	Introduction	41
3.2.	Statistical Treatment	47
3.3.	Organic Matter Richness	50
3.4.	Kerogen Classification and Thermal Maturity	52
3.5.	Organic Matter Input, Redox Conditions and Depositional Environment	58
	Conclusions	66
	References	67
	Abstract in Arabic Language	

---



## List of Tables

---

	<b>Table</b>	<b>Page</b>
Table 2.1.	Studied shales	37
Table 2.2.	Studied coals	38
Table 3.1.	Analysis of the Qahash shale	43
Table 3.2.	Analysis of the Qahash coal	43
Table 3.3.	Gas chromatogram data of normal alkanes and isoprenoids ratios of the Qahash shale	44
Table 3.4.	Gas chromatogram data of normal alkanes and isoprenoids ratios of the Qahash coal	44
Table 3.5.	Gas chromatogram data of steranes and diasteranes of the Qahash shale	45
Table 3.6.	Gas chromatogram data of steranes and diasteranes of the Qahash coal	45
Table 3.7.	Gas chromatogram data of terpanes, hopanes and TPP ratios of the Qahash shale	46
Table 3.8.	Gas chromatogram data of terpanes, hopanes and TPP ratios of the Qahash coal	46
Table 3.9.	Descriptive statistics of organic	48
Table 3.10.	Correlation matrix of organic parameters	48
Table 3.11.	Factor analysis of organic parameters	49

---

## List of Figures

<b>Figures</b>		<b>Page</b>
Figure 1.1:	Satellite image	1
Figure 1.2:	Geological map of the Cyrenaica Basin	3
Figure 1.3:	Scheme of the tectonic development of the Al Jabal Al Akhdar	4
Figure 1.4:	Stratigraphic chart of the exposed rocks in the Cyrenaica Basin	5
Figure 1.5:	Well location map of the Cyrenaica Basin	11
Figure 1.6:	Lithostratigraphic column of the sedimentary infill of the Cyrenaica Basin	13
Figure 1.7:	Lithostratigraphic column of the Qahash Formation	17
Figure 1.8:	Organic Petrographic microscope	20
Figure 1.9:	Scanning electron microscope instrument	20
Figure 1.10:	Rock-Eval 6 instrument	21
Figure 1.11:	Gas chromatography-mass spectrometry instrument	21
Figure 2.1:	Ulminite (Sample Q7)	24
Figure 2.2:	Textinite (Sample Q13)	24
Figure 2.3:	Collotellinite (Sample Q15)	25
Figure 2.4:	Telinite (Sample Q10)	25
Figure 2.5:	Densinite (Sample Q10)	26
Figure 2.6:	Attrinite (Sample Q2)	26
Figure 2.7:	Corpohuminite (Sample Q21)	27
Figure 2.8:	Gelinite (Sample Q19)	27
Figure 2.9:	Sporinite (Sample Q11)	29

Figure 2.10:	Cutinite (Sample Q14)	29
Figure 2.11:	Alginite (Sample Q11)	29
Figure 2.12:	Resinite (Sample Q14)	30
Figure 2.13:	Subernite (Sample Q19)	30
Figure 2.14:	Bituminite (Sample Q19)	31
Figure 2.15:	Fusinite (Sample Q11)	32
Figure 2.16:	Semifusinite (Sample Q11)	33
Figure 2.17:	Inertodetrinite (Sample Q15)	33
Figure 2.18:	Funginite (Sample Q13)	33
Figure 2.19:	Macrinite (Sample Q13)	34
Figure 2.20:	Micrinite (Sample Q13)	34
Figure 2.21:	Framboidal pyrite (Sample Q9)	35
Figure 2.22:	Depositional environment of the studied shales	38
Figure 2.23:	Paleoenvironmental conditions for the studied shales and coals	39
Figure 3.1:	Correlations among the analyzed organic parameters in the studied samples	49
Figure 3.2:	Plot of PC loadings of the analyzed parameters	50
Figure 3.3:	Plot of TOC vs. GP	51
Figure 3.4:	Plot of TOC vs. S <sub>2</sub>	51
Figure 3.5:	Plot of OI vs. HI	55
Figure 3.6:	Kerogen Type for the Studied Samples	56
Figure 3.7:	Plot of T <sub>max</sub> vs. HI	56
Figure 3.8:	Plot of T <sub>max</sub> vs. Ro	57
Figure 3.9:	Plot of C <sub>32</sub> 22S / (22S + 22R) Homohopane vs. C <sub>29</sub> (ββ / ββ + αα) sterane	57

Figure 3.10:	Plot of TOC vs. $S_1$	58
Figure 3.11:	Plot of Pr / Ph vs. $C_{31}R / C_{30}$ Hopane	60
Figure 3.12:	Plot of Pr / Ph vs. $(Pr + n-C_{17}) / (Ph + n-C_{18})$	60
Figure 3.13:	Plot of TPP vs. hopane / (hopanes + $\Sigma 20R$ steranes)	61
Figure 3.14:	Plot of Pr / Ph vs. WI	61
Figure 3.15:	Plot of Pr / Ph vs. CPI	62
Figure 3.16:	Plot of Pr / Ph vs. $C_{29} / C_{27}$ regular steranes	62
Figure 3.17:	Plot of Pr / Ph vs. N-Alkane SLR ( $\Sigma n-C_{12-20}$ ) / ( $\Sigma n-C_{12-29}$ )	63
Figure 3.18:	Plot of Pr / Ph vs. predominance of $C_{29}$ - components amongst diasteranes	63
Figure 3.19:	Plot of Ph / $n-C_{18}$ vs. Pr / $n-C_{17}$	64
Figure 3.20:	Ternary diagram of $C_{27}$ - $C_{28}$ - $C_{29}$ regular steranes	64
Figure 3.21:	Plot of Pr / Ph vs. G / $C_{30}$	65

---

## List of Abbreviation

Abbreviation	Meaning
API	American Petroleum Institute.
BSE	Backscattered Electron.
CPI	Carbon Preference Index.
GC-MS	Gas Chromatography-Mass Spectrometry.
GI	Gelification Index
GP	Semi-Quantitative Index.
GWI	Groundwater Index.
HI	Hydrogen Index.
OI	Oxygen Index.
PAAS	Post Archean Australian Shale.
PCA	Principal Component Analysis.
PCs	Principal Components.
PI	Production Index.
Pr / Ph	Pristane / Phytane.
Ro	Vitrinite reflectance (wt. %).
REE	Rare Earth Element.
Rr	Random reflectance.
SEM	Scanning Electron Microscope.
S <sub>1</sub>	amount of free hydrocarbons in sample (mg / g).
S <sub>2</sub>	Amount of hydrocarbons generated through thermal cracking (mg / g) – provides the quantity of hydrocarbons that the rock has the potential to produce through diagenesis.

S <sub>3</sub>	Amount of CO <sub>2</sub> (mg of CO <sub>2</sub> / g of rock) - reflects the amount of oxygen in the oxidation step.
T <sub>max</sub>	The temperature at which maximum rate of generation of hydrocarbons occurs.
TOC	Total Organic Carbon (wt. %).
TPP	Tetracyclic Polyprenoid.
TPI	Tissue Preservation Index.
VI	Visitation Index.
WI	Waxiness Index.

---

# **Organic Geochemistry of the Qahash Formation in the Offshore Well A1-NC 128, Cyrenaica Basin, NE Libya**

**By**

**OMAR ADEL OMAR GENIBER**

**Supervisor**

**Assist. Prof. Osama Shaltami**

## **ABSTRACT**

The purpose of this thesis is to characterize the organic matter content of two source rocks (shale and coal) collected from the Qahash Formation in the offshore Well A1-NC 128, Cyrenaica Basin, NE Libya. Petrographically, the studied samples are dominantly composed of Vitrinite macerals, followed by moderate Liptinite and low Inertinite macerals. However, the samples also contain a large amount of Framboidal pyrite. The TPI, GI, GWI and VI indices point towards Limno-Telmatic condition during the deposition of the shales and coals under mesotrophic to rheotrophic basin conditions. Geochemically, the Qahash Shale has a fair quality, whereas the Qahash Coal is considered as a poor source rock. Moreover, the Qahash Shale contains type II / III kerogen (mixed organic matter), while the Qahash Coal behaves as kerogens of type III and IV (Terrigenous organic matter). The organic matter is thermally immature. The Qahash Formation was deposited in a high salinity marine environment.

*Keywords: Organic Petrography, Organic Geochemistry, Source Rock, Qahash Formation, Cyrenaica Basin, Libya.*

**CHAPTER ONE**  
**INTRODUCTION**



# CHAPTER ONE

## INTRODUCTION

### 1.1. General

Libya consists of five continental basins (Cyrenaica, Sirte, Kufra, Murzuq and Ghadamis basins) as well as two offshore basins (Misratah and Sabratah basins, Fig. 1.1). The Cyrenaica Basin is located in northeastern Libya, and is considered one of the small basins in Libya. Unlike the Sirt Basin no large oil or gas discoveries have been made in the Cyrenaica Basin (Hallett and Clark-Lowes, 2016). This can be attributed to a variety of factors, but the most significant is the lack of an effective source rock. None of the three main source rocks of Libya - the Tanzuft hot shale, the Frasnian shale or the Cretaceous Sirt shale are present in the Cyrenaica Basin in a facies capable of generating significant hydrocarbons (Hallett and Clark-Lowes, 2016).

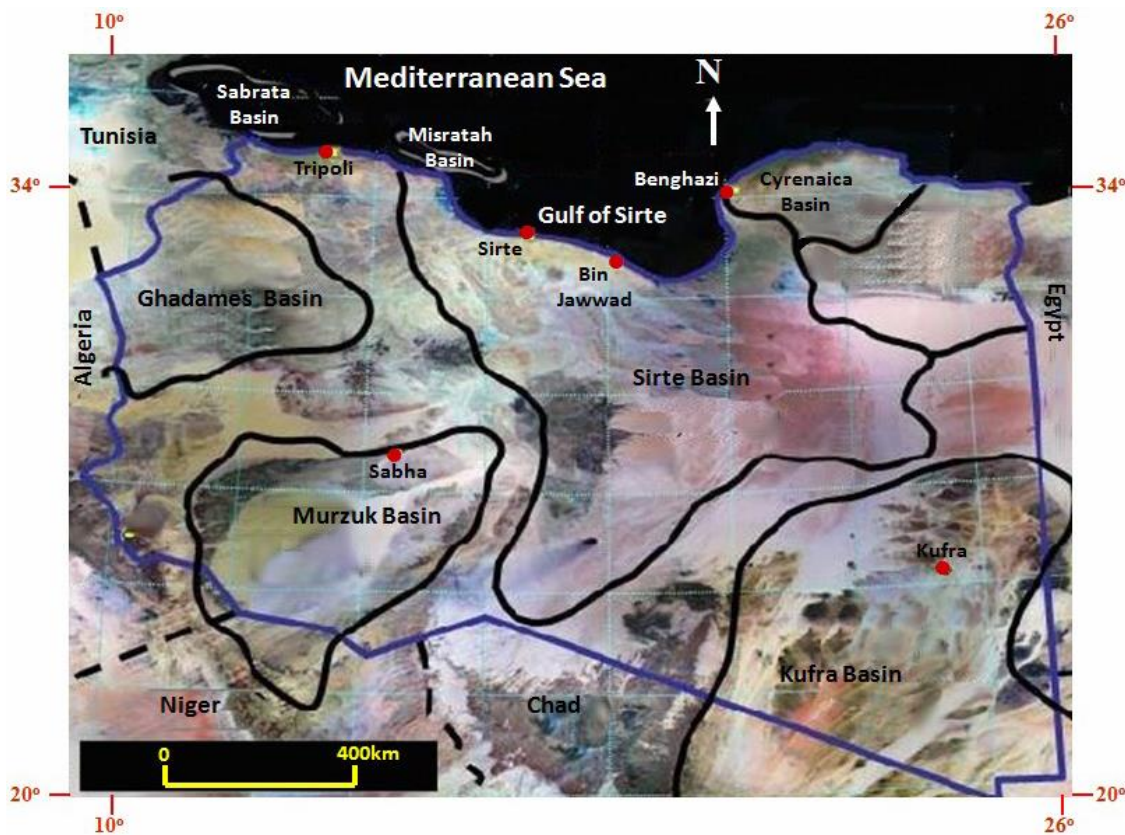


Fig. 1.1: Satellite image showing the sedimentary basins in Libya (after Shaltami, 2012).

## **1.2. Regional Geology**

The Al Jabal Al Akhdar is the largest part of the Cyrenaica Basin. It was developed at the southern margin of the Mediterranean geosynclines of the Tethys, on an attenuated continental crust of the north passive margin of the Afro-Arabian shield (El Hawat and Shelmani, 1993). The age of rocks in the Cyrenaica Basin ranges from Precambrian to Quaternary, but the exposed rocks range only from Cretaceous to Quaternary, while the rest of ages are found in the subsurface (e.g., El Hawat and Abdulsamad 2004; Hallett and Clark-Lowes, 2016, (Fig. 1.2).

### **1.2.1. Regional Structural Setting**

According to Rohlich (1980) the Late Cretaceous to Late Miocene section in the Al Jabal Al Akhdar region was described in a fashion of cyclic sedimentation stages under the influences of regional structural activities of Al Jabal Al Akhdar region (Fig. 1.3).

### **1.2.2. Regional Stratigraphic Setting**

The Cyrenaica Basin largely covered by sediments belonging to a sequence ranging from Late Cretaceous to Quaternary (Fig. 1.4). The stratigraphic sequence can be described as following:

#### **1.2.2.1. Late Cretaceous**

Previous studies (e.g., Rohlich, 1974; El Hawat and Shelmani, 1993) suggested that the Al Jabal Al Akhdar was formed during the Late Cretaceous. This age is represented by six formations (Klen, 1974; Rohlich, 1974). According to Rohlich (1974) the Al Hilal and Al Athrun formations were deposited on the coast and these formations have equivalents in the inland (Qasr Al Abid, Al Baniyah, Al Majahir and Wadi Dukhan formations). Shaltami *et al.*, (2018) found that the  $^{87}\text{Sr} / ^{86}\text{Sr}$  data suggest an age of Late Cenomanian for the Qasr Al Abid Formation, Late Turonian-Late Coniacian for the Al Baniyah, Late Santonian for the Al Hilal Formation, Middle Campanian for the Al Majahir Formation, Early Maastrichtian for the Al Athrun Formation and Late Maastrichtian for the Wadi Dukhan Formation. The new age of the Late Cretaceous formations refers to the similarity of deposition at the coast and inland.

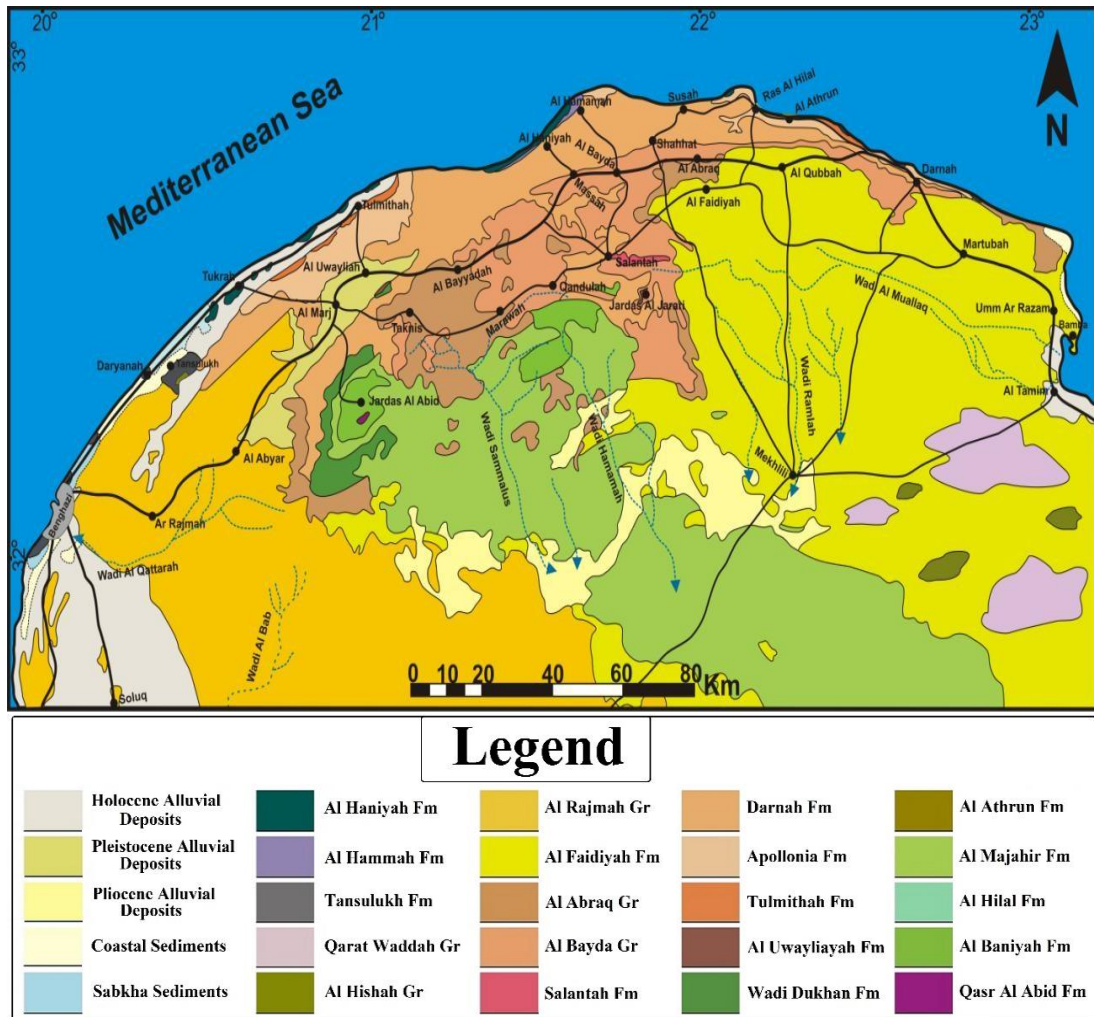


Fig. 1.2: Geological map of the Cyrenaica Basin (after Shaltami *et al.*, 2018).

### 1.2.2.2. Paleocene

The Al Uwayliyah Formation is the only rock unit representing the Paleocene epoch in the Al Jabal Al Akhdar (Rohlich, 1974). Many authors (Rohlich, 1974; El Hawat and Shelmani, 1993; El Hawat and Abdulsamad, 2004) believed that the Middle Paleocene is completely absent. The  $^{87}\text{Sr} / ^{86}\text{Sr}$  data suggest an age of Middle Danian-Middle Thanetian for the Al Uwayliyah Formation, which indicate that the Middle Paleocene is present (Shaltami *et al.*, 2018).

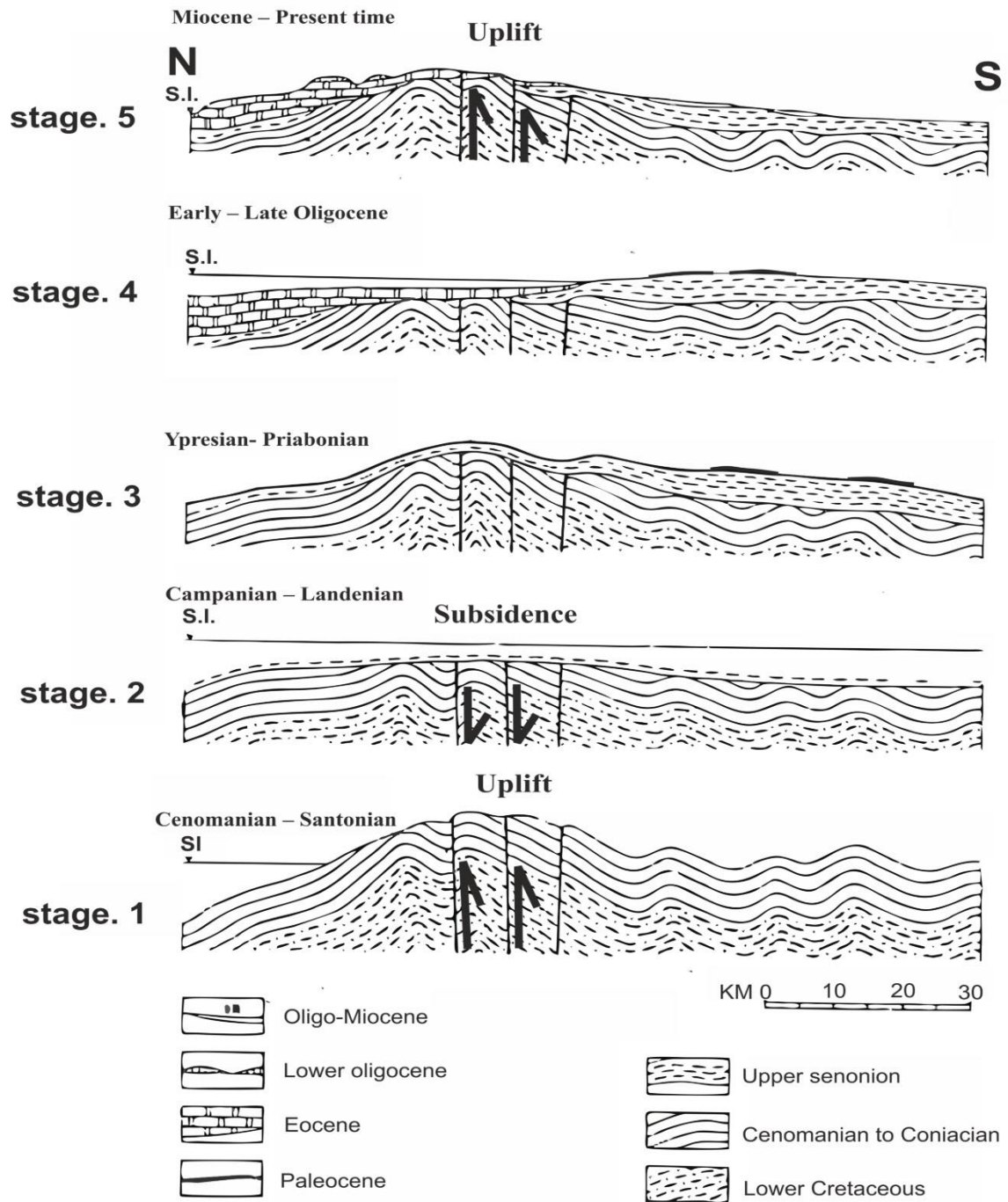


Fig. 1.3: Scheme of the tectonic development of the Al Jabal Al Akhdar (after Rohlich, 1980).

Eonothem	Erathem	System/Period	Series/Epoch	Stage/Age	Age(Ma)	Cyrenaica Basin		
<b>Phanerozoic</b>	<b>Cenozoic</b>	<b>Quaternary</b>	<b>Holocene</b>		0.0117	Coastal, Alluvial and Eolian sediments		
			<b>Pleistocene</b>	Tarantian		0.126	Al Haniyah Fm.	
				Ionian		0.781	Al Hammah Fm.	
				Calabrian		1.80	Tansulukh Fm.	
				Gelasian		2.58	Wadi Al Maqar Fm.	
			<b>Neogene</b>	<b>Pliocene</b>	Placenzian		3.60	Qarat Al Asi Fm.
					Zanclean		5.333	Uyun Ghuzayil Fm.
				<b>Miocene</b>	Messinian		7.246	Umm Al Gharaniq Fm.
					Tortonian		11.62	AL Abyar Fm. Bu Mariam Fm. Wadi Al Qattarah Fm. Al Jaghub Fm.
					Serravallian		13.82	Msus Fm.
					Langhian		15.97	Al Sceleidima Fm.
					Burdigalian		20.44	Benghazi Fm.
		Aquitanian				23.03	Jardinah Fm.	
		<b>Oligocene</b>			Chattian		28.1	Al Faidiyah Fm.
					Rupelian		33.9	Qasr Al Balatah Fm.
				<b>Eocene</b>	Priabonian		38.0	Massah Fm.
					Bartonian		41.3	Marawah Fm.
			Lutetian			47.8	Shahhat Fm.	
			<b>Paleocene</b>	Ypresian		56.0	Salantah Fm.	
		Thanetian			59.2	Darnah Fm.		
		Selandian			61.6	Apollonia Fm.		
		Danian			66.0	Tulmithah Fm.		
		<b>Late</b>		Maastrichtian		72.1	Al Uwayliayah Fm.	
				Campanian		83.6	Wadi Dukhan Fm.	
			Santonian		86.3	Al Athrun Fm.		
			Coniacian		89.8	Al Majahir Fm.		
			Turonian		93.9	Al Hilal Fm.		
			Cenomanian			Al Banyah Fm.		
								Qasr Al Abid Fm.

Fig. 1.4: Stratigraphic chart of the exposed rocks in the Cyrenaica Basin (after Shaltami et al., 2018).

### **1.2.2.3. Eocene**

Pietersz (1968) divided the Eocene deposits in the Al Jabal Al Akhdar into the Apollonia, Darnah and Salantah (or Slonta) formations. The type localities of the three formations mentioned above are situated at the Susah village, Darnah city and Salantah village, respectively (Pietersz, 1968). It is very difficult to separate the Darnah Formation from the Salantah Formation; consequently the former is incorporated within the Darnah Formation (Rohlich, 1974). It is now generally accepted that the Eocene deposits in the Al Jabal Al Akhdar are divided into two formations; a basal Apollonia Formation and an overlying Darnah Formation. It is dreadfully hard to determine the contact between these two formations, because in some areas in the Al Jabal Al Akhdar, the Apollonia Formation interfingers with the Darnah Formation (Rohlich, 1974; Hallett, 2002). Based on the fossil content, the probable depositional environment of the Apollonia Formation is the deep marine, whereas the Darnah Formation was definitely deposited in a shallow marine environment (Rohlich, 1974). Shaltami *et al.*, (2018) calculated the numeric age for the Eocene deposits in the Al Jabal Al Akhdar. This new age is as follows: 1) Early Ypresian and Late Ypresian-Early Lutetian for the lower and upper parts of the Apollonia Formation, respectively, and 2) Late Lutetian-Early Priabonian and Late Priabonian for the lower and upper parts of the Darnah Formation, respectively. Obviously, the Apollonia and Darnah formations are unquestionably separated by an unconformity, because the Middle Lutetian is missing. Furthermore, the Middle Priabonian is not present in the Darnah Formation; therefore it is necessary to separate the Darnah Formation from the Salantah Formation. Additionally, the Middle Ypresian is completely absent in the Apollonia Formation. Based on the new age and new type locality, they suggest a new name (Tulmithah Formation) for the lower part of the Apollonia Formation.

### **1.2.2.4. Oligocene**

The Oligocene in Libya marks a period of regression in which the shoreline migrated northwards (Hallett, 2002). Significant outcrops of Oligocene rocks are present in the Jabal Al Akhdar. According to Rohlich (1974) these Oligocene rocks are divided into two formations namely; the Al Bayda Formation (Early Oligocene) and Al Abraaq Formation (Late Oligocene). The name Al Bayda Formation was introduced by Rohlich (1974) and

comprises two members; the Shahhat Marl Member and Algal Limestone Member. The lithological nature and paleontological content of the formation suggest a neritic, largely shallow marine environment (Rohlich, 1974). Shaltami *et al.*, (2017) found that the Sr isotope analysis of crystalline calcites from the two members gave an age of Early Rupelian for the Shahhat Marl Member, and Late Rupelian for the Algal Limestone Member. Moreover, the K-Ar age of the fine Illites ( $< 0.2 \mu\text{m}$ ) from the Shahhat Marl Member was also defined at Early Rupelian. There is an obvious lack of the Middle Rupelian. Thus, they concluded that the sediments of the two members mentioned above are unquestionably separated by an unconformity. Accordingly, they changed the Al Bayda Formation to the Al Bayda Group, divided into Shahhat Formation (previously called Shahhat Marl Member) and Marawah Formation (formerly called Algal Limestone Member).

The name of the Al Abraç formation was established by Rohlich (1974) on the Al Abraç village. Shaltami *et al.*, (2018) found that the ages derived from strontium isotope analysis of crystalline calcites are Late Oligocene (Early Chattian and Late Chattian) for the Al Abraç Formation, which indicate that there is an unconformity surface, because the Middle Chattian is completely absent. Consequently, they changed the Al Abraç Formation to the Abraç Group. They divided this group into two formations: a basal Massah Formation and an overlying Qasr Al Balatah Formation.

#### **1.2.2.5. Miocene**

There were many local names that were used for the Miocene deposits in the Cyrenaica Basin, but now only seven formations have been recognized. These formations are Al Faidiyah, Benghazi, Al Sceidima, Msus, Wadi Al Qattarah, Qarat Mariem and Al Jaghbub formations (Hallett, 2002). The proved depositional environment for the formations is the shallow marine (e.g., Klen, 1974; Francis and Issawi, 1977; Giammarino, 1984; El Hawat and Abdulsamad, 2004). The Al Faidiyah and Ar Rajmah formations were defined by Pietersz (1968) and Klen (1974), respectively. The last author used the name Benghazi Member for the lower part of the Ar Rajmah Formation, and Wadi Al Qattarah Member for the upper part. El Hawat and Abdulsamad (2004) changed the status of the Ar Rajmah Formation to the Ar Rajmah Group, divided into the Benghazi and Wadi Al Qattarah

formations. The Al Sceleidima and Msus formations are also parts of the Ar Rajmah Group (Francis and Issawi, 1977). These formations were introduced by Francis and Issawi (1977) and Mazhar and Issawi (1977), respectively. Di Cesare *et al.*, (1963) identified the Al Jaghbub Formation in the Al Jaghbub oasis. Giammarino (1984) divided this formation into two members: a basal Wadi Al Hamim Member and an overlying Wadi Al Khali Member. The Qarat Mariem Formation is a transitional facies between the Al Jaghbub and Msus formations (Swedan and Issawi, 1977). Shaltami *et al.*, (2018) calculated the absolute age for the Miocene deposits in the Cyrenaica Basin. They found that these deposits from oldest to youngest are as follows: Al Faidiyah Formation (Middle Aquitanian), Jardinah Formation (Early Burdigalian), Benghazi Formation (Late Burdigalian-Early Serravallian), Al Sceleidima Formation (Late Serravallian), Msus Formation (Middle Tortonian), Al Jaghbub Formation (Early Messinian), Wadi Al Qattarah Formation (Middle Messinian), Bu Mariam Formation (earliest Late Messinian) and Al Abyar Formation (latest Late Messinian). They also found that the unconformity between the Wadi Al Qattarah and Bu Mariam formations marks the beginning of the MSC event in the Cyrenaica Basin. Furthermore, they have reformed the Ar Rajmah Group to include the Jardinah, Benghazi, Al Sceleidima, Msus, Al Jaghbub, Wadi Al Qattarah, Bu Mariam and Al Abyar formations.

#### **1.2.2.6. Pliocene**

Previous studies (e.g., Carmignani, 1984; El Hawatand Abdulsamad, 2004) showed that the Pliocene-Early Pleistocene sediments in the Cyrenaica Basin are represented by Qarat Weddah Formation, while Shaltami *et al.*, (2018) found that there are two formations in this age in the Cyrenaica Basin; a basal Al Hishah Formation and an overlying Qarat Weddah Formation. The Al Hishah Formation was introduced by Mijalkovic (1977) after Al Hishah village. Shaltami *et al.*, (2018) found that the isotope data gave ages of Early Zanclean and Late Zanclean for the Al Hishah Formation. Clearly there is an unconformity surface because the Middle Zanclean is not present (Shaltami *et al.*, 2018). Therefore, they changed the status of the Al Hishah Formation to the Al Hishah Group divided into the Umm Al Gharaniq and Uyun Ghuzayil formations (with names based on new type localities). The  $\delta^{30}\text{Si}$  and trace element ratios indicated that the Umm Al Gharaniq and Uyun Ghuzayil formations were deposited in fluvial and shallow marine environments, respectively (Shaltami *et al.*, 2018).



Unlike all previous studies, Shaltami *et al.*, (2018) found that the Pliocene deposits are present in the Al Jabal Al Akhdar represented by the Umm Al Gharaniq Formation. This formation represents the Zanclean flood that coincided with the end of the MSC event in the Cyrenaica Basin. There was also deposition of alluvial sediments (terra rossa soil, conglomerate and calcrete) during the Late Pliocene (Middle-Late Piacenzian) (Shaltami *et al.*, 2018).

#### **1.2.2.7. Quaternary**

The Qarat Weddah Formation was established by Di Cesare *et al.*, (1963) on the Qarat Weddah hill. The isotope data suggested two different ages (Middle-Late Piacenzian and Middle Gelasian) for the Qarat Weddah Formation (Shaltami *et al.*, 2018).

The ages derived from isotope analysis indicate the complete absence of the Early Piacenzian and Early Gelasian, indicating the presence of two unconformity surfaces. The first surface separates the Al Hishah Group and Qarat Weddah Formation and the other separates the lower and upper parts of the Qarat Weddah Formation was studied by (Shaltami *et al.*, 2018). Thus, they concluded that the Qarat Weddah Formation must be changed to the Qarat Weddah Group which can be divided into the Qarat Al Asi and Wadi Al Maqar formations. The possible depositional environments for the Qarat Al Asi and Wadi Al Maqar formations are the shallow marine and fluvial environments, respectively (Shaltami *et al.*, 2018).

On the other side Klen (1974), Rohlich (1974) and Zert (1974) showed that there are two types of the Quaternary calcarenites in the Al Jabal Al Akhdar: marine and aeolian. Shaltami *et al.*, (2017) supported this assumption by the PAAS-normalized REE patterns. They used crystalline calcite to determine the age of the calcarenites. The  $^{87}\text{Sr} / ^{86}\text{Sr}$  ratio gave an age of Early-Late Calabrian for the marine calcarenite and Middle Ionian for the lower part of the aeolian calcarenite, while the  $^{230}\text{Th} / ^{238}\text{U}$  ratio suggested a Middle-Late Tarantian age for the upper part. Obviously, there are two unconformities because the Early Ionian and Late Ionian-Early Tarantian are not present. Based on the new age and new type localities they gave names for the calcarenites (Tansulukh Formation for the marine calcarenite, while they divided the aeolian calcarenite into two formations; a basal Al Hamamah Formation and an overlying Al Haniyah Formation). According to Shaltami *et al.*, (2018) the Early Pleistocene (Middle Gelasian) is the numeric age for the tufa and travertine in the Cyrenaica

Basin. There are alluvial sediments belonging to the Late Pleistocene (Middle-Late Tarantian) (Shaltami *et al.*, 2018).

According to Shaltami *et al.*, (2018) the Early Holocene in the Cyrenaica Basin is represented by the sabkha deposits (Early-Middle Boreal) and alluvial sediments (Late Boreal). They also added that the youngest deposits in the basin are the coastal sediments (Middle Holocene (Early-Late Atlantic)).

### **1.3. Present Study**

#### **1.3.1. Qahash Formation**

The Qahash Formation was introduced by Duronio *et al.*, (1991) for subsurface sequences encountered in the AI-NC 120 and AI-NC 128 wells (Fig. 1.5). In Well AI-NC 120 the lower boundary of the Qahash Formation is conformable with the underlying Sirual Formation (Late Jurassic), and the upper boundary is conformable with the overlying the Daryanah Formation (Early Cretaceous) (Shaltami *et al.*, 2018). The formation contains rare non-diagnostic fossils, but on the basis of stratigraphic position it is believed to be Valanginian to Barremian in age (Hallett, 2002). The thickness in the well is about 200 m (Shaltami *et al.*, 2018).

In Well AI-NC 128, the lower boundary of the Qahash Formation is conformable with the underlying Mallegh Formation (Late Jurassic), and the upper boundary is covered by the Daryanah Formation (Hallett, 2002). The thickness of the formation in this well is probably more than 1500 m (Hallett, 2002). Other wells show a variety of facies from open-marine to the shallow-water sandstones and shales with gypsum found in Well B1-18 (Hallett, 2002).



### 1.3.3. Previous Work

There are many previous studies on the petroleum system of the Cyrenaica Basin. However, the source rocks and reservoirs in the basin are shown in (Fig. 1.6). The following is a summary of the preceding studies:

Based on the information obtained from the oil companies, Buitrago *et al.*, (2011) suggested the existence of three main reservoirs and two source rocks in the Cyrenaica Basin. The reservoirs are as follows: 1) The Early Cretaceous carbonates (Daryanah Formation), 2) The Late Cretaceous carbonates (Al Baniyah Formation), and 3) The Middle-Late Eocene carbonates (Darnah Formation), while the source rocks are as follows: 1) The Qasr Al Abid Formation (Late Cretaceous shales), and 2) The Al Hilal Formation (Late Cretaceous shales). They also suggested that the Qahash Shale is not considered a producer of hydrocarbons, because type IV kerogen is predominant in the shale.

Hallett and Clark-Lowes (2016) believed that there are other source rocks in the Cyrenaica Basin. These source rocks are as follows:

- 1) The Middle-Late Jurassic sediments (Sirual Formation).
- 2) The Early Cretaceous shales (Qahash and Daryanah formations).

Moreover, Hallett and Clark-Lowes (2016) found that the Qahash Shale is dominated by gas-prone type III kerogen.

Shaltami *et al.*, (2018), in two different studies, found new source rocks in the Cyrenaica Basin. These source rocks are as follows:

- 1) The Early-Middle Eocene marls (Apollonia Formation).
- 2) The Late Oligocene marls (Massah and Qasr Al Balatah formations).

reservoir quality, they used the technology of petroleum inclusions. They found the following:

Source Rock	Reservoir	Lithostratigraphy	Age
		Coastal, Alluvial and Eolian sediments	<b>Quaternary</b>
		Al Haniyah Fm.	
		Al Hamamah Fm.	
		Tansulukh Fm.	
		Wadi Al Maqar Fm.	<b>Neogene</b>
		Qarat Al Asi Fm.	
		Uyun Ghuzayil Fm.	
		Umm Al Gharaniq Fm.	
		Al Abyar Fm.	
		Bu Mariam Fm.	
		Wadi Al Qattarah Fm.	
		Al Jaghbub Fm.	
		Msus Fm.	
		Al Sceleidima Fm.	
		Benghazi Fm.	<b>Paleogene</b>
		Jardinah Fm.	
		Al Faidiyah Fm.	
		Qasr Al Balatah Fm.	
		Massah Fm.	
		Marawah Fm.	
		Shahhat Fm.	
		Salantah Fm.	
		Darnah Fm.	
		Apollonia Fm.	
		Tulmithah Fm.	<b>Cretaceous</b>
		Al Uwayliayah Fm.	
		Wadi Dukhan Fm.	
		Al Athrun Fm.	
		Al Majahir Fm.	
		Al Hilal Fm.	
		Al Baniyah Fm.	
		Qasr Al Abid Fm.	
		Daryanah Fm.	
		Qahash Fm.	
		Mallegh Fm.	<b>Jurassic</b>
		Ghurab Fm.	
		Sirual Fm.	

Fig. 1.6: Lithostratigraphic column of the sedimentary infill of the Cyrenaica Basin showing the source rocks and reservoirs (after Shaltami et al., 2019).

Furthermore, Shaltami *et al.*, (2018), in another study, conducted a geochemical assessment of the Qahash and Daryanah formations in the offshore Well Al-NC 120. To determine the

- 1) There are two different types of quality; good quality (Qahash and Daryanah shales) and poor quality (Qahash Coal).
- 2) Type II / III and III kerogen are dominant in the Qahash and Daryanah shales, while the Qahash Coal is characterized by the predominance of type IV kerogen
- 3) All organic matter in the source rocks is thermally immature.
- 4) The organic matter in the Qahash and Daryanah shales is of mixed type, while the Qahash Coal contains terrigenous organic matter.
- 5) In general, the Daryanah Reservoir is characterized by immature oil.
- 6) There are indications of oil-water interactions in the petroleum inclusions.
- 7) The Qahash and Daryanah shales are the main source rocks of the Daryanah Reservoir.
- 8) The hydrocarbons were charged to the Daryanah Reservoir in two different times.

Additionally, Shaltami *et al.*, (2019) conducted eight different studies on the petroleum system of the Cyrenaica Basin. The following is a summary of these studies:

**First study:** They conducted a geochemical study of reservoirs in the Cyrenaica Basin to determine the types of natural gases using petroleum inclusions. They found the following:

- 1) The petroleum inclusions show a slight difference in the homogenization temperature, and
- 2) Generally, the Daryanah Reservoir inclusions are characterized by high concentration of hydrocarbon gases (especially C<sub>1</sub>) and low concentration of non-hydrocarbon gases (H<sub>2</sub>, H<sub>2</sub>S, CO<sub>2</sub> and N<sub>2</sub>). The opposite is true for the inclusions of the Al Baniyah and Darnah reservoirs.

**Second study:** They discovered the existence of a petroleum system in Al Bayda Group (the Shahhat Formation represents the source rock while the reservoir represented by the Marawah Formation).

**Third study:** They evaluated the crude oil in the Al Baniyah Reservoir using petroleum inclusions. They found the following: 1) The petroleum inclusions contain two oil families,

2) The characteristics of the Family I oils indicate that these oils were sourced from the Late Santonian shale (Al Hilal Formation), while the Late Cenomanian marl (Qasr Al Abid Formation) is the probable source for the Family II oils, 3) All the studied oils are thermally immature, and 4) Two episodes of oil charging took place in the Al Baniyah Reservoir.

**Fourth study:** They conducted a geochemical evaluation of organic matter in the Miocene deposits of the Cyrenaica Basin. They found the following: 1) The shales and marls display three grades of organic richness, namely good (Al Faidiyah and Benghazi shales), fair (Al Faidiyah Marl and Al Sceleidima Shale) and poor (Benghazi Marl, Sceleidima Marl, Msus Shale, Msus Marl and Al Jaghbub Marl), 2) The Al Faidiyah and Benghazi shales are characterized by kerogen of type II, while the rest of the samples contain kerogen of type II / III and III, 3) All shales and marls contain immature organic matter, except for the Al Faidiyah and Benghazi shales, 4) Migrated hydrocarbons are dominant in the Al Faidiyah and Benghazi shales, while other sediments contain generated hydrocarbons, and 5) The Al Sceleidima and Al Jaghbub samples are characterized by terrigenous organic matter, whereas mixed organic matter is prevailing in the other samples. They also designed new models that can be used to determine the origin and type of organic matter as well as the depositional environment.

**Fifth study:** They evaluated the petroleum inclusions in the Miocene limestones and sandstones of the Cyrenaica Basin. They found the following: 1) The Benghazi Formation is the only Miocene reservoir in the Cyrenaica Basin, 2) There are two genetically distinct oil families in the Benghazi Reservoir inclusions, 3) All oil families are thermally mature, 4) Based on the API gravity values, the studied samples are classified as medium to heavy oils, 5) The crude oils are of condensate type, 6) The Middle Aquitanian shale (Al Faidiyah Formation) and the Late Burdigalian-Early Serravallian shale (Benghazi Formation) are the main sources of the Benghazi Reservoir oils, and 7), There are two different charging times took place in the Benghazi Reservoir.

**Sixth study:** They studied the changes in trace element, bulk organic, and biomarker inventories archived in sediments of the Al Uwayliyah Formation. They found the

following: 1) The compositions of organic matter repeatedly changed in the Al Uwayliayah Formation, varying from kerogen type-III in the limestones, to type-II in the marls, 2) The Al Uwayliayah Marl can be considered a good source rock (TOC > 1%), while the quality of the Al Uwayliayah Limestone ranges from poor to fair (TOC < 1%), 3) The Al Uwayliayah Formation contains immature to early mature organic matter, 4) The presence of rearranged diasterenes suggests enhanced clay catalysis rather than thermal catalysis, and 5) The Al Uwayliayah Marl was deposited under the influence of episodic photic zone anoxia. On the other hand, a fully oxidized photic zone was present during the deposition of the Al Uwayliayah Limestone.

**Seventh study:** They conducted oil-oil and oil-source rock correlations for the Eocene deposits (Apollonia and Darnah formations) in the Cyrenaica Basin. They found the following: 1) The quality of the Apollonia Marl (source rock) ranges from good to excellent, 2) The Apollonia Marl contains type - II kerogen, 3) There is one oil family in the petroleum inclusions of the Darnah Reservoir; this oil is of medium type, 4) The Darnah Reservoir oils were derived from the Apollonia Marl, and 5) The samples of crude oils and source rock have entered in the oil generation window.

**Eighth study:** They evaluated the petroleum system of the Pliocene deposits in the Cyrenaica Basin. They found the following: 1) The TOC contents indicated that the Uyun Ghuzayil Shale is a fair source rock, while the Uyun Ghuzayil Diatomite has a good quality, 2) The source rocks have diverse potential ranging from gas-prone to oil-prone, 3) The organic matter is thermally immature and characterized by the sovereignty of type II / III and III kerogens, 4) Land-plant derived organic matter is dominant in the diatomite and shale samples with a small contribution of marine organic matter, 5) The Uyun Ghuzayil Diatomite is the main source rock of the Umm Al Gharaniq Reservoir oils, whereas the Qarat Al Asi Reservoir oils were derived from the Uyun Ghuzayil Shale, 6) Based on the API gravity values, the Umm Al Gharaniq and Qarat Al Asi reservoirs contain medium and heavy oils, respectively. These oils are thermally immature, and 7) The most abundant gas in the reservoirs is C<sub>1</sub> with lesser amounts of C<sub>2</sub>, C<sub>3</sub>, nC<sub>4</sub>, iC<sub>4</sub>, N<sub>2</sub>, CO<sub>2</sub> and H<sub>2</sub>S.



### 1.3.4. Stratigraphy

Figure (1.7) shows the lithostratigraphic column of the Qahash Formation in the offshore Well Al-NC 128. The total thickness is about 1500 m. In this well, the lower boundary of the Qahash Formation is conformable with the underlying Mallegh Formation (Late Jurassic), and the upper boundary is covered by the Daryanah Formation (Early Cretaceous).

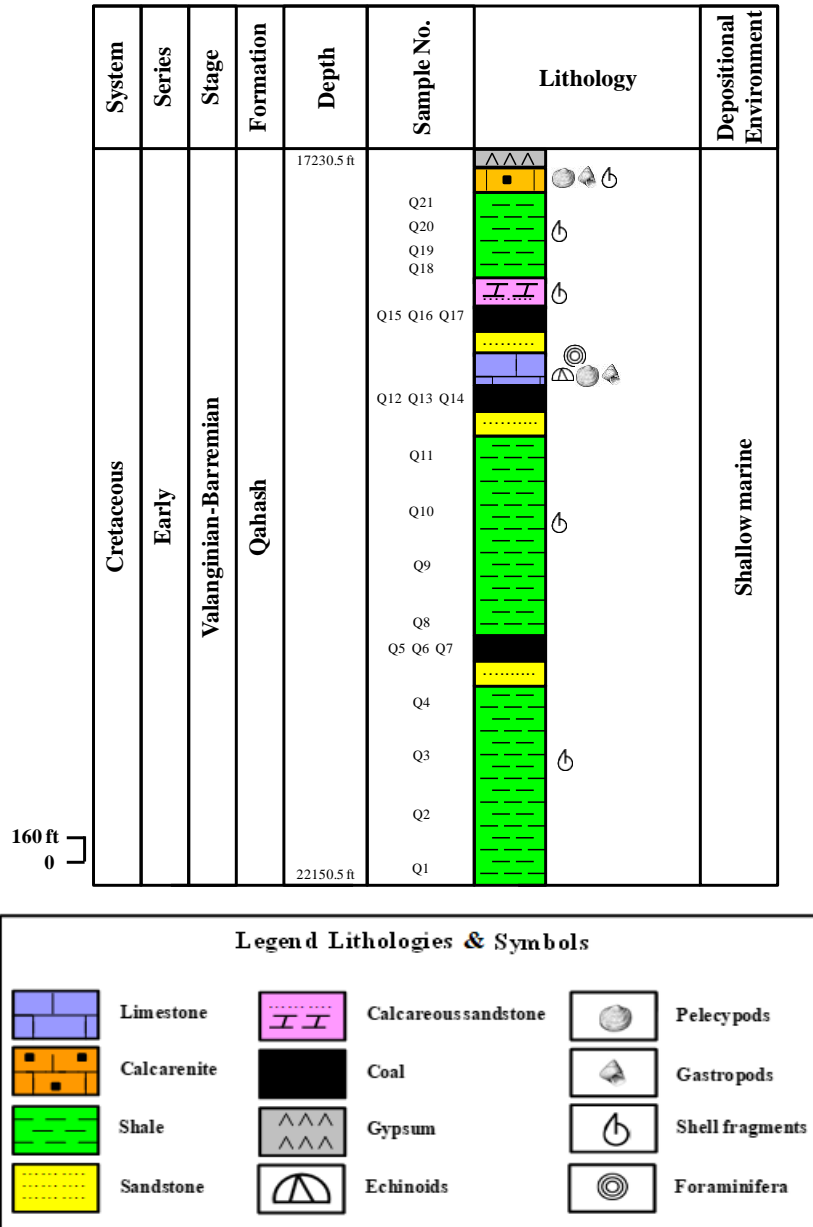


Fig. 1.7: Lithostratigraphic column of the Qahash Formation in the offshore Well Al-NC 128.

### **1.3.5. Methodology**

#### **1.3.5.1. Sampling**

The data used in this work was obtained from the AGIP Company. Twelve samples of shale and nine samples of coal were selected (Fig. 1.7). All analyses used in the current study were carried out in the laboratory of Chemostratigraphy and Organic Geochemistry (LGQM), State University of Rio de Janeiro (UERJ), Brazil.

#### **1.3.5.2. Organic Petrography**

To define the type of macerals in the studied samples, the organic petrographic microscope (Fig. 1.8) was used in this study. For the petrographical analysis, specifications of ISO 7404-2 (2009) were followed. Maceral analyses and reflectance measurements were carried out as per ISO 7404-3 (2009) and ISO 7404-5 (2009) standards, respectively. The maceral analysis was carried out on Leica DM 4500P microscope, simultaneously under normal incident and fluorescence (blue light excitation; to help with liptinite identification and distinction) under an oil immersion objective (50 x). For maceral analysis, 500 counts for each sample were done using the software Petroglite 2.35. The reflectance measurements (100 readings / sample) were made on maceral huminite using Sapphire (0.594 % Ro) as standard, immersion oil with a refractive index of 1.518, a photometry system (PMT III) and evaluated using the software MSP 200.

#### **1.3.5.3. Scanning Electron Microscope (SEM)**

The scanning electron microscope (Fig. 1.9) was used to identify some types of macerals. For SEM imaging, rock-chip samples were mounted onto aluminum stubs using Crystalbond™ 509 as an adhesive. The mounted samples were then mechanically polished with sandpaper at a progressively smaller grit size to 1500 grit, using water as a polishing fluid. The polished samples were ion milled with argon using continuous rotational motion in a Fischione 1060 SEM Mill for 3h at 5 kV with an incidence angle of 2°. To reduce charging effects in the SEM, samples were minimally coated with Au / Pd using a Denton Vacuum Desk V sputter coating system. A backscattered electron (BSE) detector was chosen for imaging. The accelerating voltage in the SEM was altered depending on the information

desired with 25 kV accelerating voltage primarily used to increase contrast for differentiating between macerals.

#### **1.3.5.4. Rock Eval Pyrolysis**

The pyrolysis analysis has been carried out using Rock-Eval-6 pyrolysis technique (Fig. 1.10). Pyrolysis results were represented by different parameters such as volatile hydrocarbons ( $S_1$  peak) liberated at temperature less than  $300^\circ\text{C}$  and the pyrolytic hydrocarbons ( $S_2$  peak) released during the temperature programmed pyrolysis in the range  $300 - 600^\circ\text{C}$ . The  $S_1$  and  $S_2$  are expressed in milligrams of hydrocarbons per gram of rock (mg/g). “ $S_3$ ” peak represents the quantity of  $\text{CO}_2$  formed by pyrolysis of the organic matter and expressed in milligrams of  $\text{CO}_2$  per gram of rock (mg / g). Total organic carbon (TOC) is the sum of the pyrolyzed carbon and residual carbon. The hydrogen index is the normalized hydrogen content of a rock sample and is calculated as:  $\text{HI} = S_2 \times 100 / \text{TOC}$ ; the oxygen index is the normalized oxygen content of a rock sample and is calculated as:  $\text{OI} = S_3 \times 100 / \text{TOC}$ ; the production index is calculated:  $\text{PI} = S_1 / (S_1 + S_2)$ .

#### **1.3.5.5. Gas Chromatography-Mass Spectrometry (GC-MS)**

Saturated and aromatic fractions of rock extracts were analyzed by gas chromatography–mass spectrometry (GC-MS, Fig. 1.11) to determine molecular composition. GC-MS was carried out using an Agilent 7890 gas chromatograph linked to an Agilent 5975C mass spectrometer ( $30\text{ m} \times 0.25\text{ mm i.d.} \times 0.25\ \mu\text{m}$ ), equipped with a film Zebron-ZB1 fused silica column used with He as the carrier gas at  $35\text{ m/s}$ . The oven temperature was initiated at  $80^\circ\text{C}$  and programmed to increase at a rate of  $3^\circ\text{C/min}$  to  $310^\circ\text{C}$ , where it was held for 5 min. The source temperature was  $200^\circ\text{C}$ . For quantitative analysis, calculation of peak areas from selected ion chromatograms was performed.



*Fig. 1.8: Organic Petrographic microscope.*



*Fig. 1.9: Scanning electron microscope instrument.*



*Fig. 1.10: Rock-Eval 6 instrument.*



*Fig. 1.11: Gas chromatography-mass spectrometry instrument.*

**CHAPTER TWO**  
**ORGANIC PETROGRAPHY**

# CHAPTER TWO

## ORGANIC PETROGRAPHY

### 2.1. Introduction

Coal is a heterogeneous natural substance consisting of a number of constituents. Microscopically basic coal constituent is maceral which is synonymous to minerals in inorganic rocks (Tayler and Cook, 1962; Diessel, 1992; Kruszewska, 2003). However, there is a difference between mineral and maceral. Minerals are generally inorganic crystalline in nature and has got a definite chemical composition, whereas a maceral is a noncrystalline organic substance and its composition may vary widely (Van Krevelen, 1993). Inorganic substances like mineral matter, shale, clay, and silt are also inherent constituents of coal (Sengupta, 2013). These constituents are recognized by the morphology, texture, and gray level or reflectance of macerals (Van Krevelen, 1993). Macerals are classified into three major organic groups, viz., Vitrinite / Huminite, Liptinite / Exinite, and Inertinite, and one inorganic group, i.e., shale + Mineral matter (Kruszewska, 2003). Association of macerals constitutes microlithotype. These constituents are classified based on mono-, bi-, or tri- assemblage of the constituents (Kruszewska, 2003).

Further subdivision of individual maceral groups is done based on physical and optical characters which include structure and texture, morphology, mode of occurrence, gray value / reflectance, etc. Definition of macerals for bituminous coals was first brought out in the International Handbook of Coal Petrology in 1963. Since then it was felt necessary to update the definitions by ICCP. As a result, a new nomenclature of the Vitrinite group of macerals was evolved (ICCP System 1994a, b).

Maceral group – defined by level of reflectance.

Maceral subgroup – defined by degree of destruction.

Maceral – defined by morphology and degree of gelification.

## 2.2. Vitrinite Group

Vitrinite is a coalification product of humic substances which essentially originates from the tissues of roots, stems, barks, and leaves composed of lignin and cellulose. Depending on the process of decomposition, degree of gelification, and rank, cell structures are preserved in Vitrinite. Color and reflectance of Vitrinite change progressively with rank. Transformation of vegetable tissues is set in successive stages, namely, Humification, Gelification, and Vitrinization (Stach, 1982). The most significant processes of Vitrinite formation from precursors are Humification and Gelification. Humification involves slow progressive oxidation, which may be accelerated by addition of oxygen. In the presence of oxygen, the lignin is first attacked by Wooddestroying fungi and then aerobic bacteria and is converted into humic substance (Sengupta, 2013).

Vitrinite group includes a group of macerals whose color is gray and whose reflectance is generally between that of the associated darker Liptinites and brighter Inertinites over the rank range in which three respective maceral groups can be readily recognized (Sengupta, 2013). The term Huminite in low-rank coal, i.e., Lignite or brown coal, is synonymous to Vitrinite in medium- to high rank coal (Stach, 1982). Vitrinite group embraces three subgroups, namely telovitrinite, detrovitrinite and gelovitrinite.

In the present study, the Vitrinite is the dominant maceral group in both shales and coals. The detected Vitrinites are as follows:

- 1) Telovitrinite (ulminite, textinite, collotelinite and telinite, (Figs. 2.1-2.4).
- 2) Detrovitrinite (densinite and attrinite, (Figs. 2.5-2.6).
- 3) Gelovitrinite (corpohuminite and gelinite, (Figs. 2.7-2.8).

The shales contain high content of detrovitrinite with lesser amount of telovitrinite and gelovitrinite, whereas the coals are high in telovitrinite. Both telinite and collotelinite exist in the form of persistent bands, while ulminite and textinite occur as a mottled vitrinitic groundmass binding other coal components. Both densinite and attrinite is composed of commonly round, vesicled to non-vesicled, and equant to elongate bodies without obvious plant structure with high reflectance. Gelinite is homogeneous and structureless infilling of



cracks and other voids. Corpohuminite is distinguished from Vitrinites by a characteristic bright oval or circular morphology.

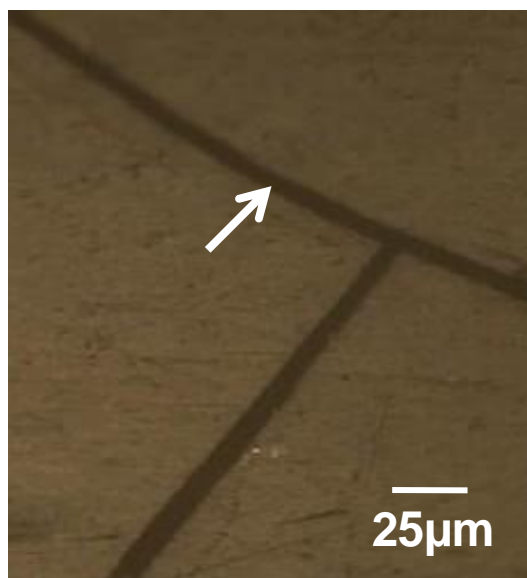


*Fig. 2.1: Photomicrograph showing ulminite (white arrow, sample Q7).*

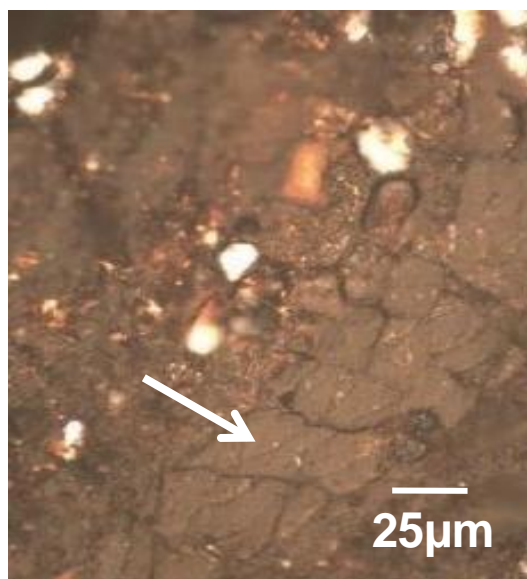


*Fig. 2.2: Photomicrograph showing textinite (white arrow, sample Q13).*

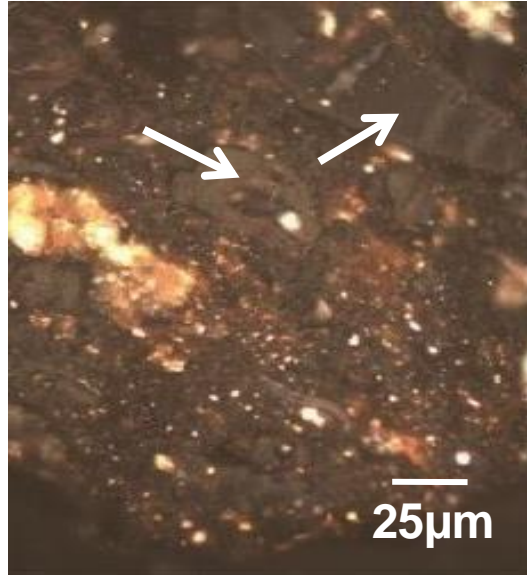


*Fig. 2.3: Photomicrograph showing Collotellinite (white arrows, sample Q15).*

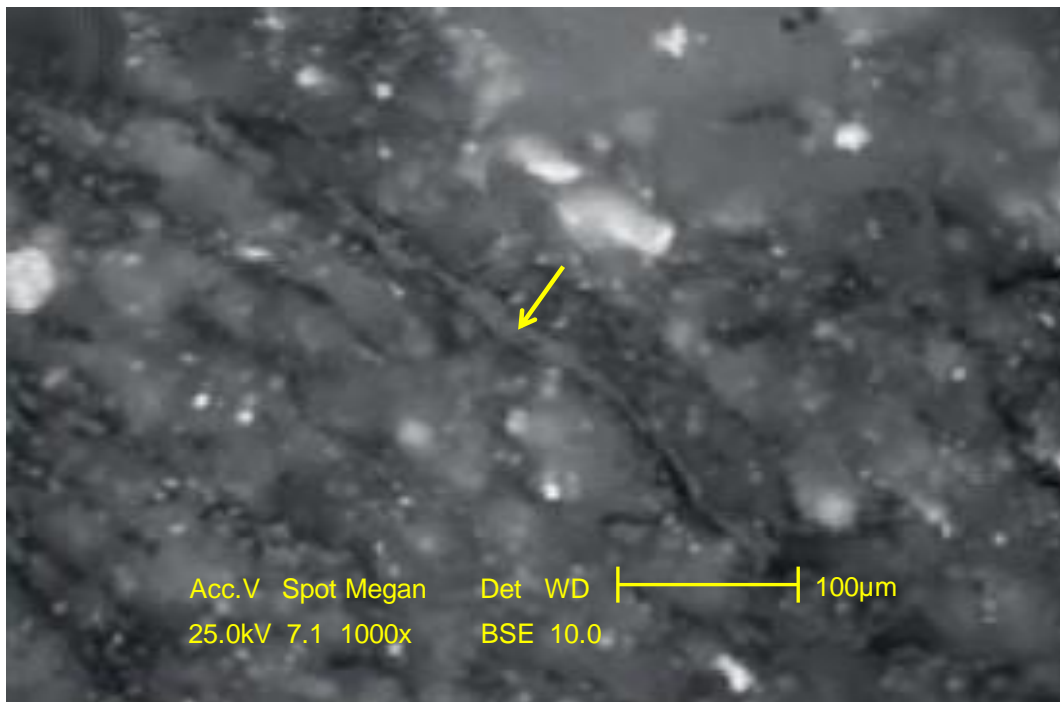


*Fig. 2.4: BSE image showing telinite (yellow arrow, sample Q10).*

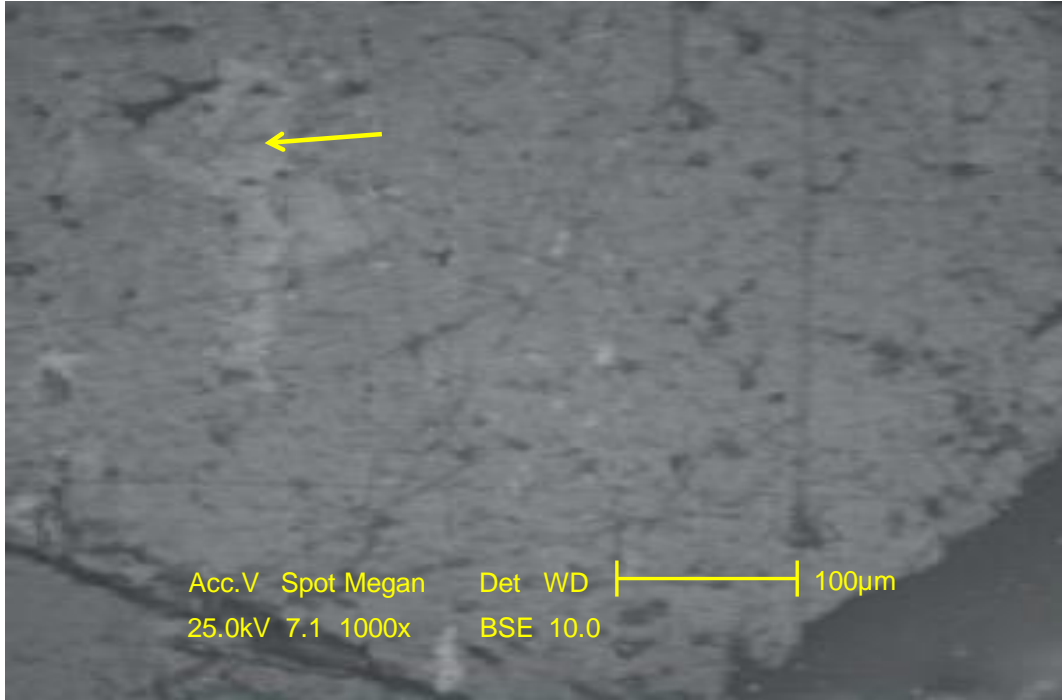


*Fig. 2.5: BSE image showing densinite (yellow arrow, sample Q10).*

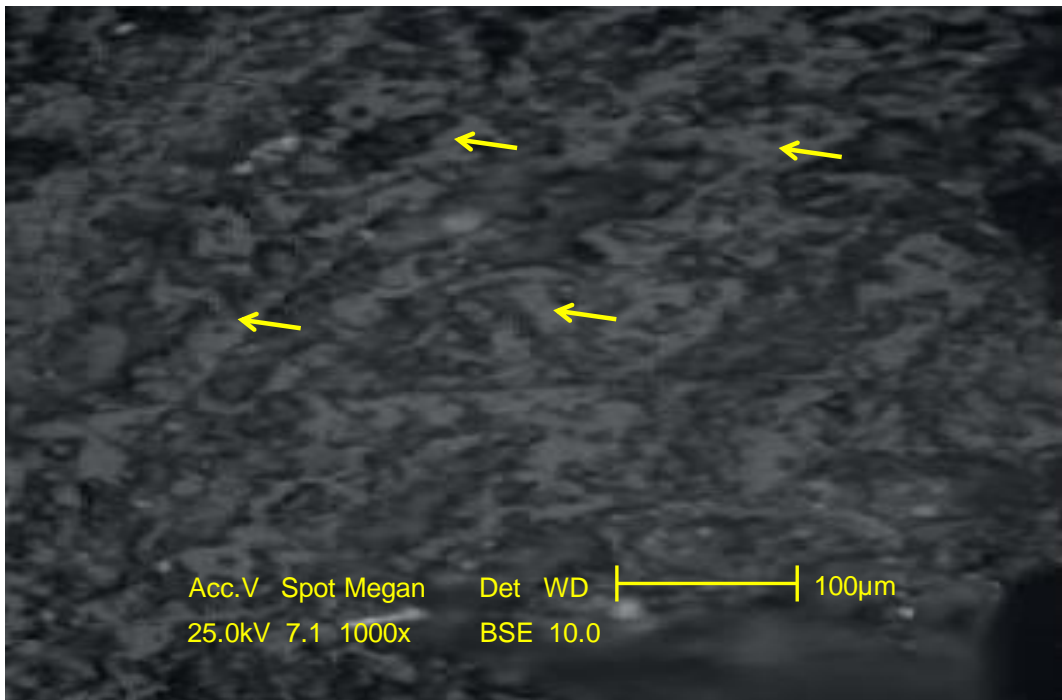


*Fig. 2.6: BSE image showing attrinite (yellow arrows, sample Q2).*

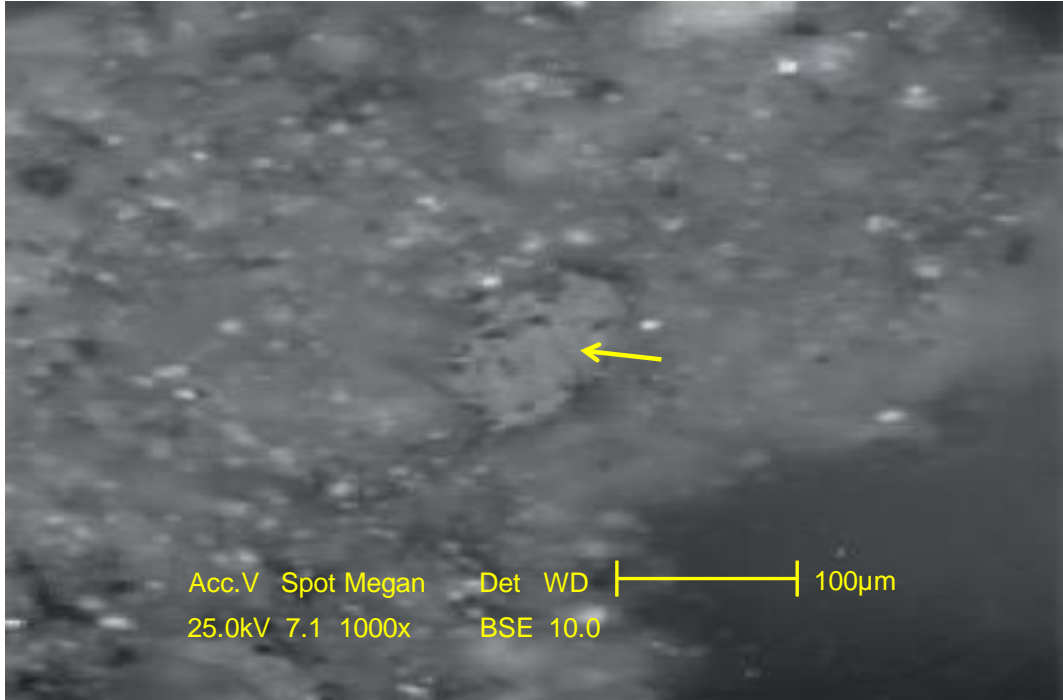


*Fig. 2.7: BSE image showing corpohuminite (yellow arrow, sample Q21).*

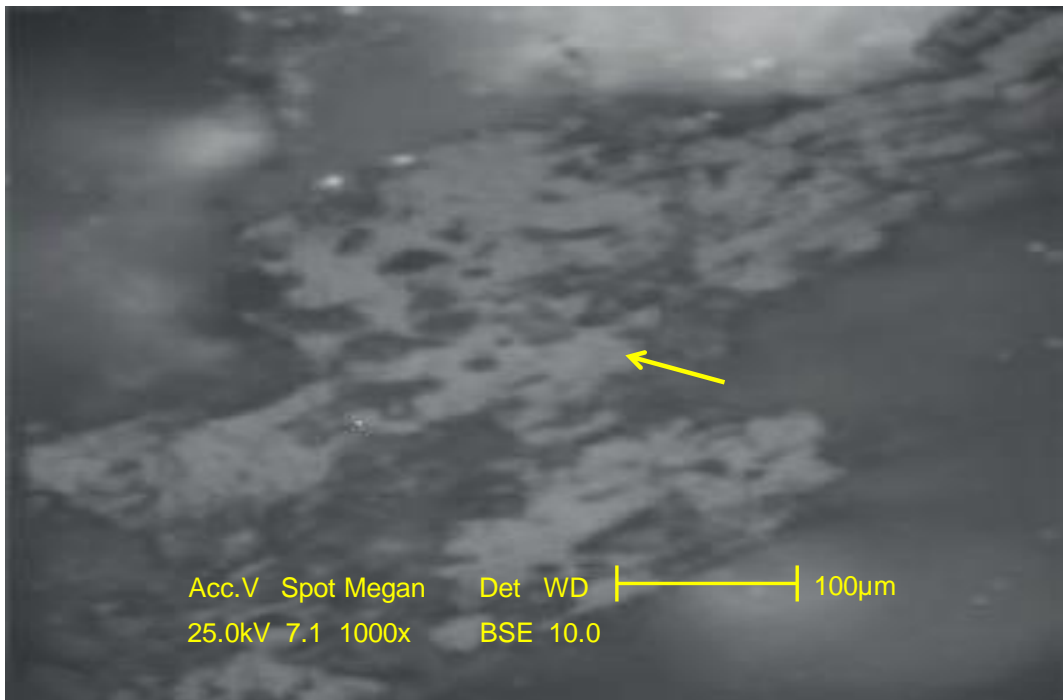


*Fig. 2.8: BSE image showing gelinite (yellow arrow, sample Q19).*

### **2.3. Liptinite Group**

It originates from relatively hydrogen-rich plant material, viz., spore, pollen, resin, cutin, suberin, wax, balsam, latex, fat, and oil, as well as from bacterial degradation products of protein, cellulose, and other carbohydrates. It has got strong fluorescence property (Stach, 1982).

Some of its members like alginite, cutinite, sporinite, and suberinite have considerable paleoenvironmental significance. Moreover, Liptinite group contributes in coke formation (Van Krevelen, 1993). Generally liptinite contents are small in Gondwana coal, but high hydrogen content within it influences the technological properties of coal. There are two major groups of liptinite: 1) Primary Liptinites, and 2) Secondary Liptinites.

In the current study, the liptinite group is represented by primary Liptinites (sporinite, cutinite, alginite, resinite and subernite, (Figs. 2.9-2.13) with sporadic secondary Liptinites (Bituminite, Fig. 2.14). Resinite is the most common liptinite macerals. The occurrence of resinite as cell fillings indicates that at some point in the maturation process, the resinite was relatively fluid. Under fluorescence mode, resinite displays pale to bright yellow color. Cutinite occurs as thin gray lenticular bands under normal reflected light and exhibits yellowish color with lower intensity under fluorescence mode. Suberinite occurs as layers of cell walls. It shows a weak reddish fluorescence color. Sporinite occurs as a skin of spores and pollen. Most of the spores are flattened and compressed in morphology. Thin-walled as well as thick-walled spores are common in the studied samples. Alginite has a characteristic shape of round and oval bodies. It is dark gray under normal reflected light and shows greenish yellow color under fluorescence mode. Bituminite occurs as fine-grained groundmass that appears as veinlets. Under reflected light, it is dark brown to dark grey in color.

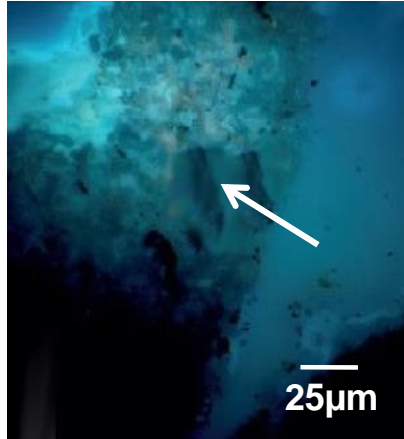


*Fig. 2.9: Photomicrograph (oil immersion) showing sporinite (white arrow, Sample Q11).*

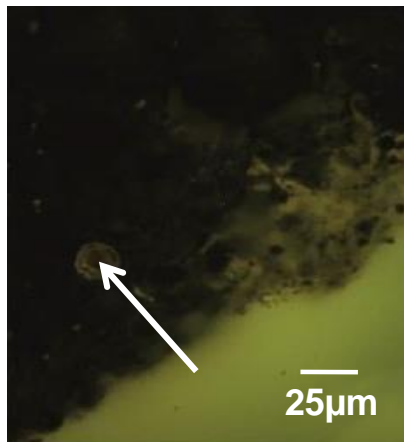


*Fig. 2.10: Photomicrograph showing cutinite (white arrow, sample Q14).*

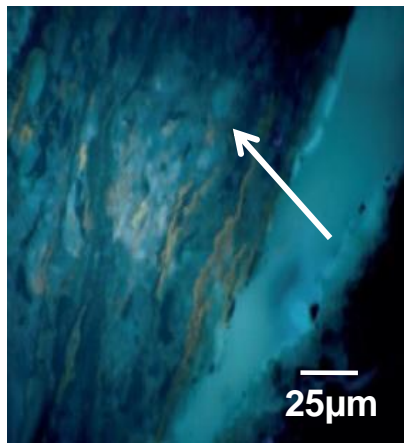


*Fig. 2.11: Photomicrograph (oil immersion) showing alginite (white arrow, sample Q11).*



*Fig. 2.12: Photomicrograph showing resinite (white arrow, sample Q14).*

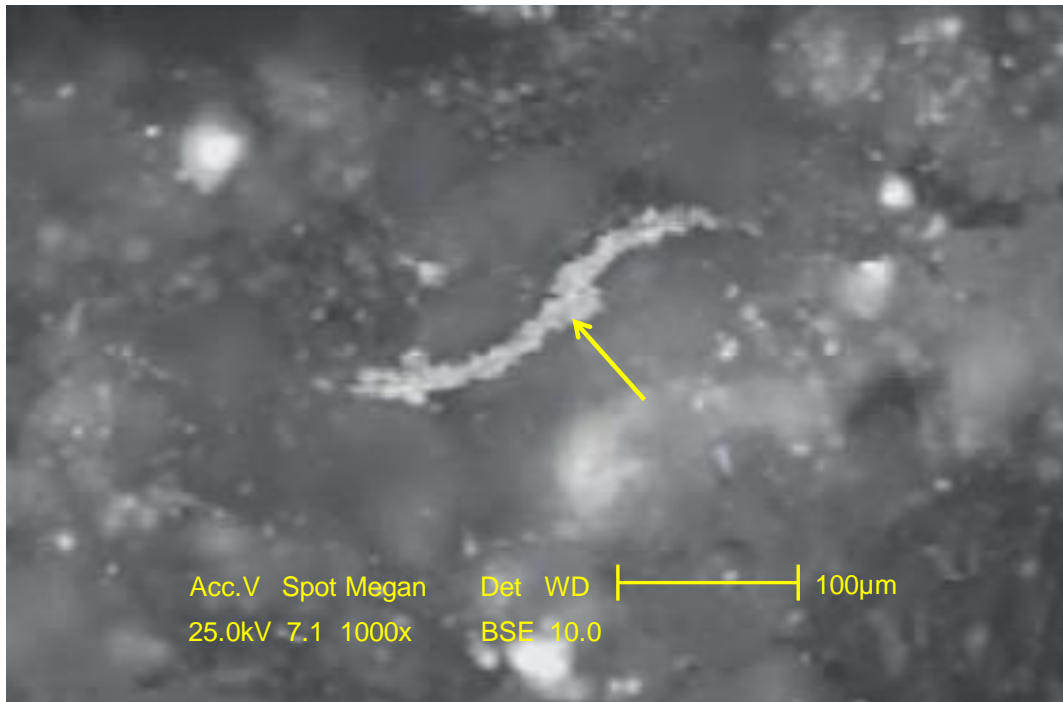


*Fig. 2.13: BSE image showing subernite (yellow arrow, sample Q19).*

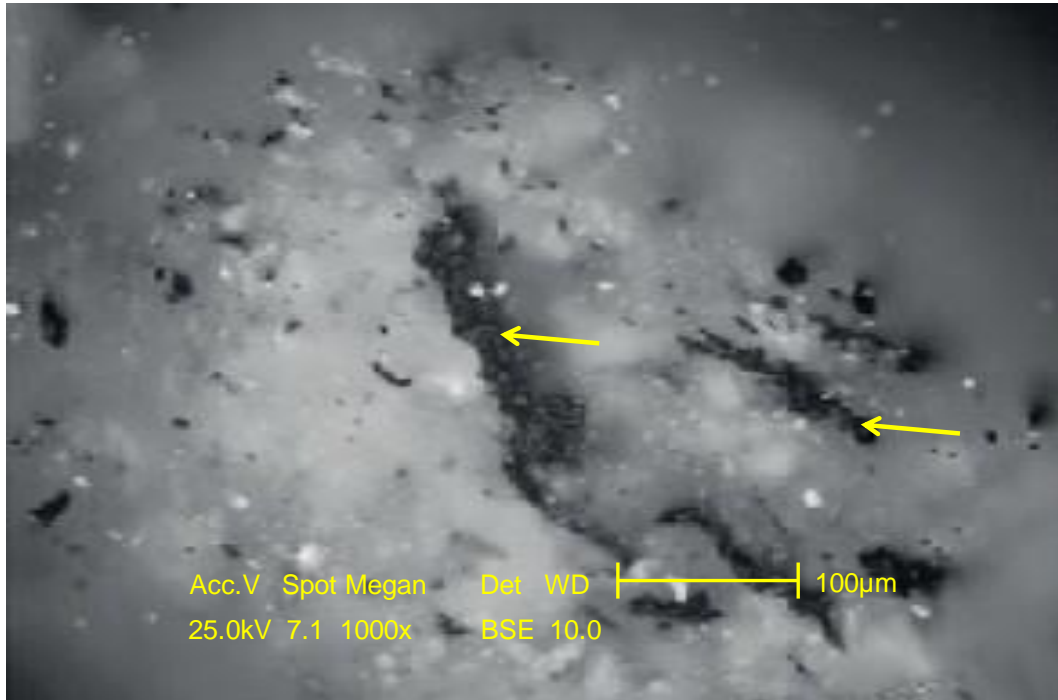


*Fig. 2.14: BSE image showing bituminite (yellow arrows, sample Q19).*

## **2.4. Inertinite Group**

Inertinite is a maceral group that comprises macerals whose reflectance in low- and medium rank coals and in sedimentary rocks of corresponding rank is higher in comparison to the macerals of the Vitrinite and Liptinite groups (Stach, 1982). The Inertinite group of macerals originates from the same plant constituents as of Vitrinite that are altered and degraded under oxidizing condition before deposition or by biochemical processes at the peat stage. They exhibit higher degree of aromatization and condensation. Chemical composition of Inertinite suggests higher carbon and lower oxygen and hydrogen content compared to Vitrinite (Van Krevelen, 1993). On the basis of plant cell structure and morphology, seven macerals are classified under Inertinite group (Van Krevelen, 1993). These macerals are as follows:

- 1) Fusinite.
- 2) Semifusinite.
- 3) Funginite.
- 4) Secretinite.
- 5) Macrinite.



6) Micrinite.

7) Inertodetrinite.

In the studied samples, the Inertinite group is recorded in the lowest concentration, and is constituted of fusinite, semifusinite, inertodetrinite, funginite, macrinite and micrinite (Figs. 2.15-2.20). Funginite is characterized by single and multi-celled fungal spores (teleutospores) and as oval and elliptical bodies (fungal sclerotia), is well represented. Fusinite is mostly derived relic tissues and cellular structures and is commonly well-preserved with yellow color. The cell lumens in semifusinite are only vague or partially visible. The cell lumens vary in size and shape even in the same particle, but they are generally smaller than those of the corresponding tissues in fusinites. Inertodetrinite is represented by small fragments derived by the physical degradation of the other types of Inertinite, most probably fusinite and semifusinite. Macrinite occurs either as an amorphous matrix or as discrete, structureless bodies of variable shapes. Micrinite exists as very small rounded grains. Aggregates of micrinite differ from macrinite by their granularity.

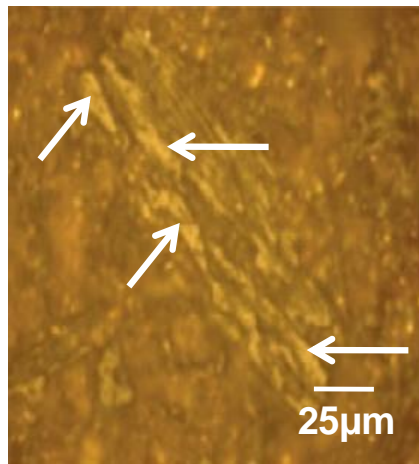


*Fig. 2.15: Photomicrograph (oil immersion) showing fusinite (white arrows, sample Q11).*

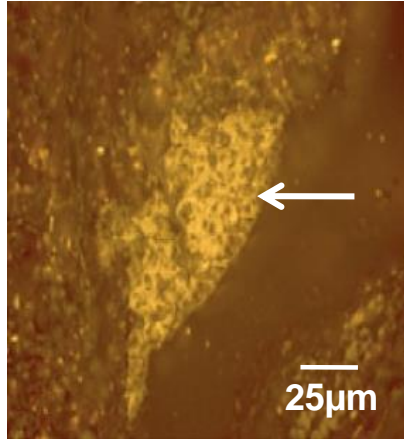


*Fig. 2.16: Photomicrograph (oil immersion) showing semifusinite (white arrow, sample Q11).*

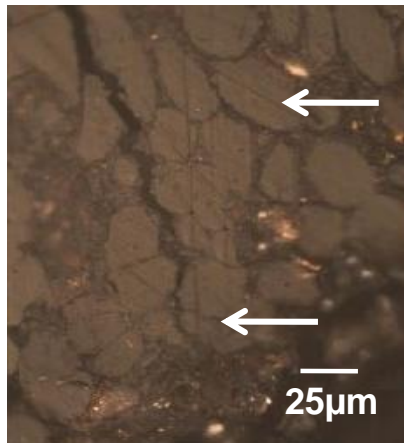


*Fig. 2.17: Photomicrograph showing inertodetrinite (white arrows, sample Q15).*

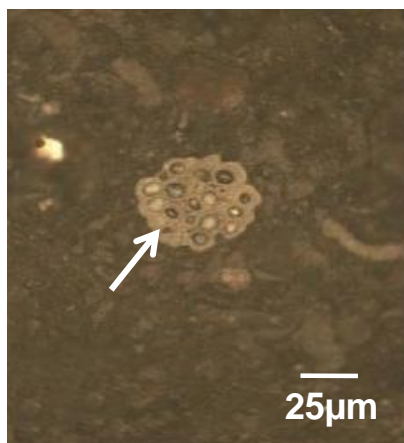


*Fig. 2.18: Photomicrograph showing funginite (white arrow, sample Q13).*

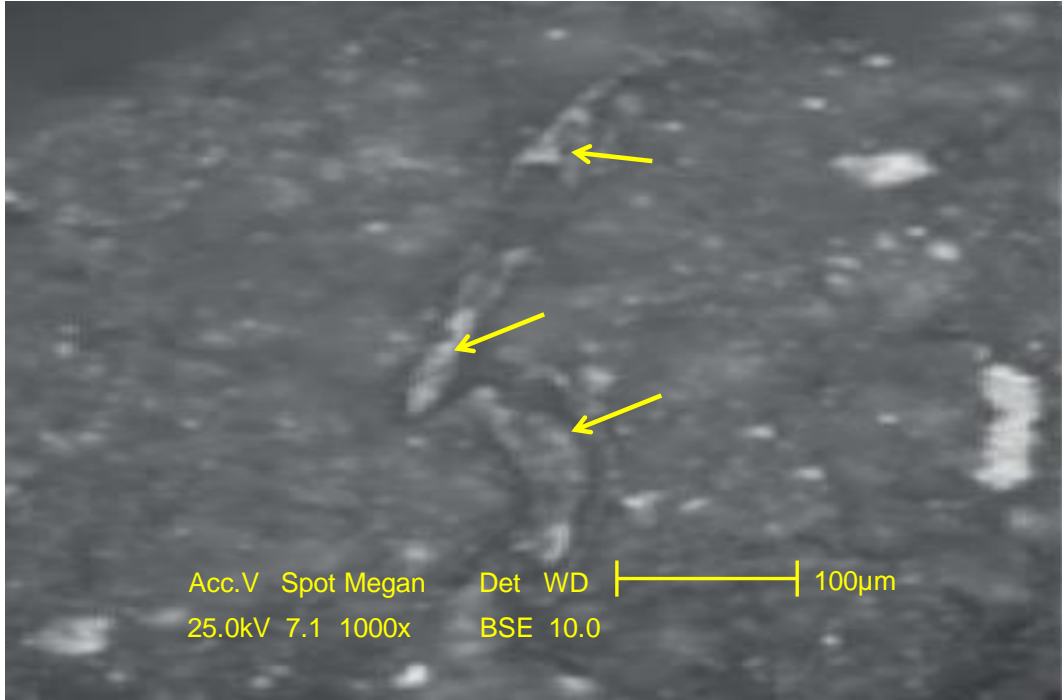


*Fig. 2.19: BSE image showing macrinite (yellow arrows, sample Q13).*

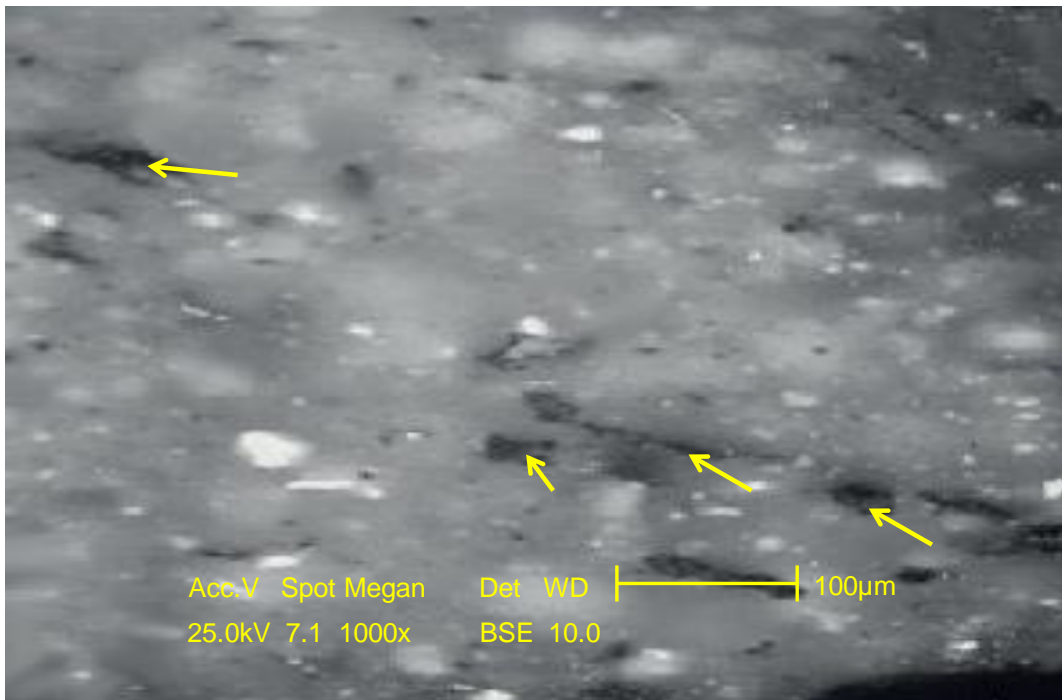


*Fig. 2.20: BSE image showing micrinite ((yellow arrows, sample Q13).*

## 2.5. Mineral Matter

The mineral matter is mainly represented by framboidal pyrite (Fig. 2.21). The term framboid describes a micromorphological feature common to certain sedimentary minerals, particularly pyrite (Ohfuji and Rickard, 2005). Framboidal structure comprises roughly spherical aggregates of discrete equi-regular euhedral microcrystallites of around 0.5  $\mu\text{m}$  in diameter, with the average aggregate size ranging from 5-20  $\mu\text{m}$  (Wilkin and Barnes, 1997). Framboid diameter tends to correlate positively with microcrystal size, and microcrystal packing is most commonly irregular and disordered (Ohfuji and Rickard, 2005). According to Wilkin and Barnes (1997) pyrite framboid formation may be the result of four consecutive processes:

- 1) Nucleation and growth of initial iron monosulfide microcrystals.
- 2) Reaction of the microcrystals to greigite ( $\text{Fe}_3\text{S}_4$ ).
- 3) Aggregation of uniformly sized greigite microcrystals, i.e., framboid growth.
- 4) Replacement of greigite framboids by pyrite.

In anoxic environments, which are typical of deeper strata, the hydrogen sulfide ( $\text{H}_2\text{S}$ ) needed for the formation of iron sulfides is produced by biogenic reduction of sulfate ( $\text{SO}_4^{2-}$ ), either by degradation of organic matter or by oxidation of methane ( $\text{CH}_4$ ) (Garman *et al.*, 2005).

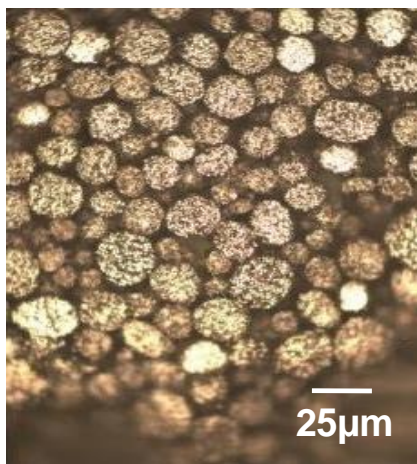


Fig. 2.21: Photomicrograph showing framboidal pyrite (sample Q9).

## 2.6. Maceral Indices

The maceral indices used in the identification of the depositional facies and environment, include gelification index (GI), tissue preservation index (TPI), groundwater index (GWI) and vegetation index (VI). The GI and TPI indices were originally formulated by Diessel (1986), whereas the GWI and VI indices were instituted by Calder *et al.*, (1991). The GI, TPI, GWI and VI were later modified by Kalaitzidis *et al.*, (2000). Although contrasting views exist (e.g., Crosdale, 1993; Wust *et al.*, 2001), the GI and TPI concept is generally used to define the paleodepositional conditions (Lamberson *et al.*, 1991; Flores, 2002; Suarez-Ruiz *et al.*, 2012; Singh *et al.*, 2019). However, a more valid result can be obtained by multidisciplinary approaches (Moore and Shearer, 2003).

The GI is the ratio of gelified versus non-gelified macerals, and indicates the wetness in peatforming environment (Flores, 2002). High GI value is indicative of a high moisture/water level and higher subsidence rate and vice versa (Singh *et al.*, 2017). The TPI measures the degree of humification of the peatforming organic matter (Lamberson *et al.*, 1991). A high TPI value ( $> 1$ ) reflects equilibrium between the growth and accumulation of plant materials, rise of the water table, and domination of tree vegetation. A low TPI suggests either predominance of herbaceous plants in the mire or large-scale degradation of plant tissues as a result of advanced humification (Diessel, 1986). The TPI also indicates the pH conditions of paleomires because in a low pH conditions, microbial activity is weak and plants can be well preserved, and vice-versa (Zhang *et al.*, 2010). The GWI indicates the level of ground water (and relative rainfall) during the peat accumulation (Calder *et al.*, 1991). Mires are usually formed in successive variations between rheotrophic, mesotrophic and ombrotrophic hydrological conditions (Amijaya and Littke, 2005; Silva *et al.*, 2008). A low GWI value ( $< 0.5$ ) indicates ombrotrophic hydrological conditions, whereas high values ( $> 1$ ) indicate rheotrophic hydrological conditions (Kalaitzidis *et al.*, 2000). A mesotrophic hydrological condition is characterized by values in between 0.5 and 1 (Kalaitzidis *et al.*, 2000). The VI is related to the type of vegetation that dominated the mire (Calder *et al.*, 1991). It is dependent on the type of peat-forming plant communities (e.g. trees and bushes). The following formulas were adopted from Kalaitzidis *et al.*, (2000) to calculate the indices of the studied samples:

$GI = (\text{Ulminite} + \text{Corpohuminite} + \text{Gelinite} + \text{Densinite}) / (\text{Textinite} + \text{Attrinite} + \text{Inertinite}).$

$TPI = (\text{Ulminite} + \text{Textinite} + \text{Corpohuminite} + \text{Fusinite}) / (\text{Attrinite} + \text{Densinite} + \text{Gelinite} + \text{Inertodetrinite}).$

$GWI = (\text{Corpohuminite} + \text{Gelinite} + \text{Densinite} + \text{Mineral Matter}) / (\text{Textinite} + \text{Ulminite} + \text{Attrinite}).$

$VI = (\text{Ulminite} + \text{Textinite} + \text{Resinite} + \text{Subernite} + \text{Fusinite}) / (\text{Attrinite} + \text{Densinite} + \text{Inertodetrinite} + \text{Cutinite} + \text{Sporinite} + \text{Alginite} + \text{Bituminite}).$

The GI, TPI, GWI and VI values for the studied samples listed in (Tables 2.1-2.2) and extrapolated in (Figs. 2.22-2.23). Clearly, the gelification index is higher in the shales than that of the coals. Likewise, the tissue preservation, vegetation and ground water indices are lower in the shales than those of the coals.

## 2.7. Rank of Coal

Rank (maturity) of the studied coals is determined by reflectance measurement on ulminite (vitrinite) maceral. The mean random reflectance (Rr) value ranges from 0.24 to 0.29 %; suggesting that the studied coals have attained brown coal (German Standard) or lignitic stage / rank (ASTM) and is of low rank B (ISO: 11760, 2005), and fall in the early diagenetic zone of methane generation (Taylor *et al.*, 1998).

Table 2.1: Maceral indices of the studied shales

Sample No.	TPI	GI	VI	GWI
Q1	0.41	2.58	0.33	0.60
Q2	0.45	3.07	0.29	1.50
Q3	0.38	2.89	0.20	0.93
Q4	0.22	2.78	0.41	0.77
Q8	0.27	3.19	0.39	1.13
Q9	0.36	2.60	0.34	0.88
Q10	0.26	3.33	0.25	0.80
Q11	0.38	3.10	0.31	0.69
Q18	0.44	2.54	0.19	1.00
Q19	0.40	2.80	0.33	1.19
Q20	0.32	2.75	0.30	0.62
Q21	0.26	2.66	0.30	0.71

Table 2.2: Maceral indices of the studied coals

Sample No.	TPI	GI	VI	GWI
Q5	0.63	1.25	0.80	1.58
Q6	0.69	1.67	0.75	2.77
Q7	0.66	1.34	0.77	3.00
Q12	0.71	1.70	0.77	2.61
Q13	0.80	1.61	0.81	3.13
Q14	0.77	1.45	0.69	1.90
Q15	0.73	1.71	0.71	1.87
Q16	0.69	1.73	0.65	1.78
Q17	0.70	1.44	0.89	2.09

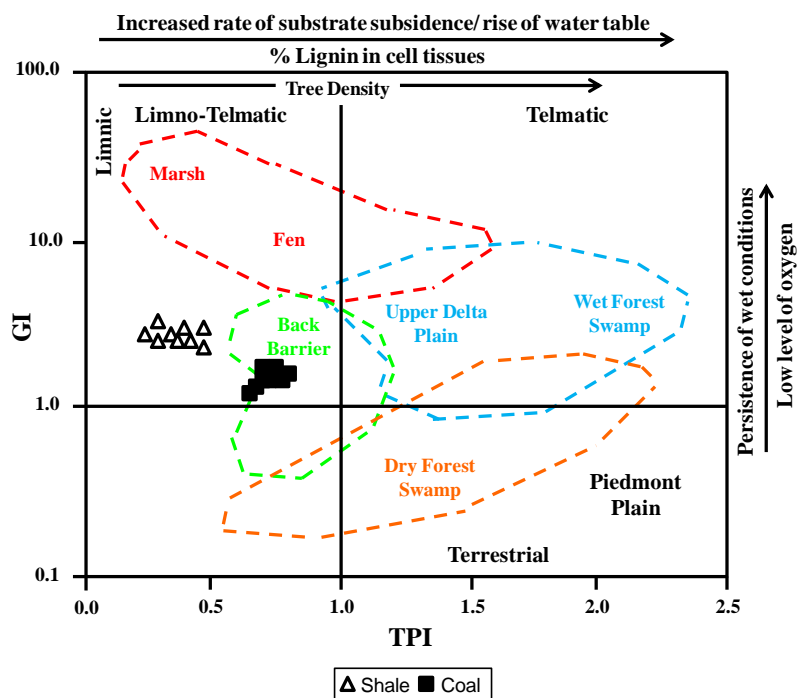


Fig. 2.22: Plot of TPI vs. GI showing the depositional environment of the studied shales and coals (fields after Diessel, 1992).

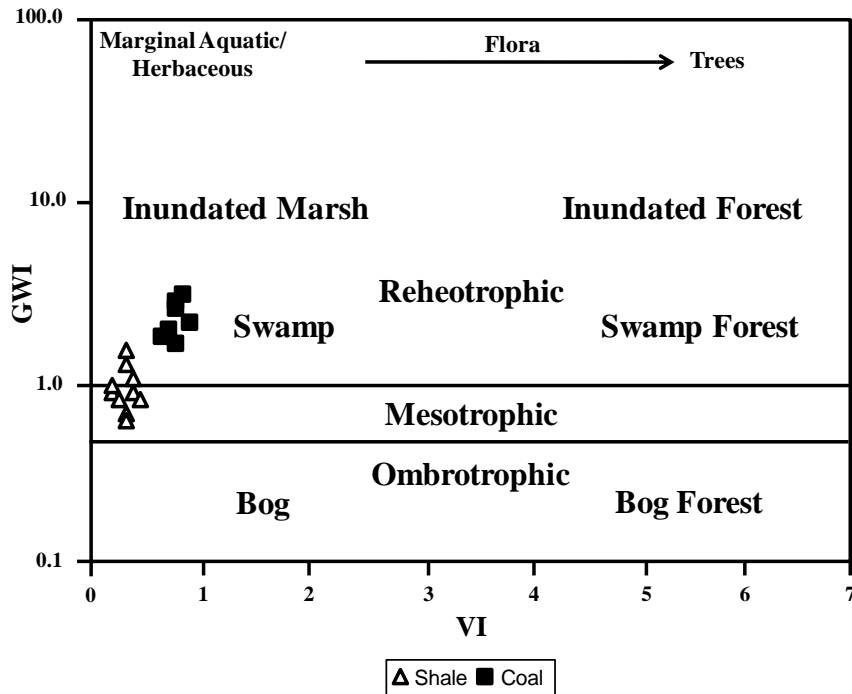


Fig. 2.23: Plot of VI vs. GI showing the paleoenvironmental conditions for the studied shales and coals (fields after Calder *et al.*, 1991).

## 2.8. Paleovegetation, Paleoclimate and Depositional Environment

The specific chemical and physical conditions existing in different depositional environment, in which organic matter accumulates, may show varying maceral and mineral matter contents (Diessel, 1992; Taylor *et al.*, 1998). However, use of organic petrography data in conjunction with other disciplines such as palynology and organic geochemistry can give a better view of the depositional environments (Scott, 2002; Suarez-Ruiz *et al.*, 2012).

In the present study, the visual organic matter analyses show the dominance of Vitrinites and subordinate amount of Liptinites; indicating woody forest vegetation inhabited in the depositional setting. The presence of funginite and sporinite indicates deposition in warm and humid climatic conditions. Generally, the studied samples are characterized by a low TPI and moderate GI values suggesting that the shales and coals were deposited in a limno-telmatic condition (Figs. 2.22-2.23). Moreover, the low TPI values indicate the high degree of degradation of organic matter. Additionally, the frequent occurrence of funginite in maceral composition suggests the intense bacterial activity. In the coals, TPI and VI values



are marginally higher than those of the shales; indicating an increased vegetation input. This is consistent with the high telovitrinite content in the coals. The high GWI values ( $> 1$ ) indicates reotrophic conditions existed in the basin during the formation of the coals, whereas mesotrophic to reheotrophic conditions existed during the formation of the shales. Frequent association of early diagenetic pyrite (framboidal) in the studied samples, formed by the bacterial reduction of sulfates, indicates the brackish water (marine) influence during the formation of the shales and coals. Therefore, it can be assumed that the Qahash Formation was deposited at the coastal setting (shallow marine environment).

**CHAPTER THREE**  
**ORGANIC GEOCHEMISTRY**

# CHAPTER THREE

## ORGANIC GEOCHEMISTRY

### 3.1. Introduction

Fine-grained rock rich in organic matter capable of generating petroleum in commercial quantities given the proper temperature and pressure is called source rock (Marshall *et al.*, 2002; Hakimi *et al.*, 2010 and He *et al.*, 2019). Source rocks can be originated in different paleo-environments such as deep marine, lacustrine and deltaic (Sykes and Snowdon, 2002; Suarez-Ruiz *et al.*, 2012; Asahina and Suzukia, 2019). Among others, shales and carbonates rocks are the sedimentary rocks which can become good petroleum source rocks (Mukhopadhyay, 1997; Ramos, 2015). Shales rocks may contain less than 5 % TOC, whereas carbonates source rocks may contain as much as 10 to 30 % TOC (Palacas, 1988).

Three main aspects are to be taken into account when characterizing a source rock: the amount and type of organic matter present at any given time, and the thermal maturity (Carvajal-Ortiz and Gentzis, 2015; El-Khadragy *et al.*, 2019). A proper evaluation of the source rocks is crucial to reach the hydrocarbons reservoirs (Ramos, 2015).

Four types of source rocks can be found in terms of petroleum generation potentiality, namely effective, active, inactive and spent (Ramos, 2015). Firstly, a potential source rock can be any rock that contains sufficient organic matter to generate petroleum (Suarez-Ruiz *et al.*, 2012). An effective source rock is a potential source rock which has reached an adequate thermal maturity to generate petroleum (Ramos, 2015). When a source rock is generating and expelling hydrocarbons either biological or by temperature at the critical moment; it is called active (Ramos, 2015). An inactive source rock might show petroleum potential but it stopped generating oil and gas (Suarez-Ruiz *et al.*, 2012). Finally, a spent source rock reached postmaturity stage and might generate wet or dry gas, but it cannot generate any oil (Suarez-Ruiz *et al.*, 2012).

Physical, biochemical and geological processes are behind the creation of a source rock, resulting in the formation of a fine-grained sedimentary rock rich in organic matter, mainly carbon and hydrogen elements (McCarthy *et al.*, 2011). A few phases need to be taken into account when a source rock is formed such as production, accumulation and preservation of the organic matter (Mackenzie, 2005). Thus, the amount and type of organic matter found in a source rock are subjected to environmental and depositional conditions. Biological activities take part in the production and transformation of organic matter. On the other hand, depositional conditions develop the concentration of the organic matter and finally the post-depositional conditions preserve it (Ramos, 2015).

Concentration and preservation of organic matter in the sediments are controlled mainly by oxygen and energy levels. Low oxygen or anoxic environment improves the preservation of organic matter, creating reducing environments which protect organic materials from oxidation and the action of bottom feeders, which implies the absence of bioturbation (Tissot and Welte, 1984). Generally, source rocks are formed in low-energy environments (Ramos, 2015).

Equally important is the mineralogy role in the source rock development. Minerals, which are transported and precipitated in the sediments, might react with organic compounds and dilute a portion of organic matter, affecting the source rock ability to generate and expel hydrocarbons (McCarthy *et al.*, 2011).

The purpose of this chapter is to characterize the organic matter content of the shales and coals of the Qahash Formation using Rock-Eval pyrolysis and GC-MS techniques. The data obtained from these techniques are listed in (Tables 3.1-3.8).

*Table 3.1: Rock Eval pyrolysis data of the Qahash Shale*

Sample No.	TOC	T <sub>max</sub>	Ro	S <sub>1</sub>	S <sub>2</sub>	S <sub>3</sub>	HI	OI	GP	PI
Q1	0.67	420	0.51	3.62	2.43	1.05	362.69	156.72	6.05	0.60
Q2	0.62	423	0.50	3.33	2.29	1.13	369.35	182.26	5.62	0.59
Q3	0.88	422	0.50	3.00	2.17	1.11	246.59	126.14	5.17	0.58
Q4	0.72	422	0.47	2.97	2.00	1.17	277.78	162.50	4.97	0.60
Q8	0.70	417	0.44	2.88	2.00	1.18	285.71	168.57	4.88	0.59
Q9	0.70	421	0.49	3.11	1.94	1.00	277.14	142.86	5.05	0.62
Q10	0.75	421	0.37	3.05	1.92	0.96	256.00	128.00	4.97	0.61
Q11	0.81	418	0.40	4.07	2.12	0.91	261.73	112.35	6.19	0.66
Q18	0.82	419	0.40	4.00	2.08	0.90	253.66	109.76	6.08	0.66
Q19	0.82	418	0.52	4.00	2.16	0.90	263.41	109.76	6.16	0.65
Q20	0.77	414	0.44	2.91	1.95	1.00	253.25	129.87	4.86	0.60
Q21	0.69	416	0.48	3.13	2.05	1.00	297.10	144.93	5.18	0.60

*Table 3.2: Rock Eval pyrolysis data of the Qahash Coal*

Sample No.	TOC	T <sub>max</sub>	Ro	S <sub>1</sub>	S <sub>2</sub>	S <sub>3</sub>	HI	OI	GP	PI
Q5	0.37	413	0.23	0.31	0.29	0.70	78.38	189.19	0.60	0.52
Q6	0.37	413	0.29	0.23	0.21	0.75	56.76	202.70	0.44	0.52
Q7	0.22	411	0.31	0.20	0.20	0.49	90.91	222.73	0.40	0.50
Q12	0.24	414	0.24	0.22	0.23	0.55	95.83	229.17	0.45	0.49
Q13	0.33	412	0.27	0.19	0.22	0.76	66.67	230.30	0.41	0.46
Q14	0.26	414	0.29	0.12	0.17	0.57	65.38	219.23	0.29	0.41
Q15	0.29	414	0.32	0.24	0.18	0.68	62.07	234.48	0.42	0.57
Q16	0.27	412	0.28	0.25	0.19	0.62	70.37	229.63	0.44	0.57
Q17	0.27	412	0.26	0.21	0.18	0.60	66.67	222.22	0.39	0.54

Table 3.3: Gas chromatogram data of normal alkanes and isoprenoids ratios of the Qahash Shale (calculated on  $m/z$  85)

Sample No.	Pr/Ph	(Pr+n-C <sub>17</sub> )/ (Ph+n-C <sub>18</sub> )	Pr/n-C <sub>17</sub>	Ph/n-C <sub>18</sub>	$\frac{\sum(n-C_{12}-n-C_{20})/}{(\sum(n-C_{12}-n-C_{20})+ \sum(n-C_{12}-n-C_{29}))}$	CPI	WI
Q1	1.61	0.57	1.00	0.97	0.60	1.17	0.50
Q2	1.44	0.61	1.10	0.90	0.57	1.05	0.61
Q3	1.55	0.43	1.12	0.94	0.55	1.11	0.66
Q4	1.57	0.49	1.10	1.00	0.48	1.10	0.54
Q8	2.09	0.40	1.05	0.88	0.51	1.10	0.63
Q9	2.33	0.40	1.00	0.91	0.47	1.05	0.52
Q10	2.61	0.62	1.00	0.94	0.50	1.09	0.52
Q11	1.10	0.44	1.17	0.96	0.54	1.10	0.82
Q18	1.89	0.62	1.18	1.00	0.54	1.14	0.66
Q19	1.70	0.62	1.09	0.89	0.44	1.20	0.69
Q20	2.00	0.73	1.05	0.97	0.50	1.12	0.69
Q21	1.63	0.70	1.00	0.95	0.50	1.10	0.71

Table 3.4: Gas chromatogram data of normal alkanes and isoprenoids ratios of the Qahash Coal (calculated on  $m/z$  85)

Sample No.	Pr/Ph	(Pr+n-C <sub>17</sub> )/ (Ph+n-C <sub>18</sub> )	Pr/n-C <sub>17</sub>	Ph/n-C <sub>18</sub>	$\frac{\sum(n-C_{12}-n-C_{20})/}{(\sum(n-C_{12}-n-C_{20})+ \sum(n-C_{12}-n-C_{29}))}$	CPI	WI
Q5	3.44	0.88	1.46	0.45	0.29	1.50	0.81
Q6	3.78	0.67	1.33	0.40	0.33	1.44	0.84
Q7	3.31	0.87	1.30	0.39	0.38	1.62	0.90
Q12	3.13	0.45	1.28	0.33	0.22	1.67	0.88
Q13	3.16	0.81	1.31	0.36	0.27	1.60	0.92
Q14	3.37	0.73	1.25	0.34	0.25	1.43	0.90
Q15	3.60	0.96	1.34	0.29	0.27	1.59	0.86
Q16	3.25	0.90	1.29	0.30	0.31	1.48	0.82
Q17	3.28	0.87	1.22	0.25	0.28	1.64	0.80

Table 3.5: Gas chromatogram data of steranes and diasteranes of the Qahash Shale  
(calculated on  $m/z$  217)

Sample No.	C <sub>27</sub>	C <sub>28</sub>	C <sub>29</sub>	C <sub>29</sub> ( $\beta\beta/\beta\beta+\alpha\alpha$ )	C <sub>29</sub> $\beta\alpha$ (S+R)-dia/ (C <sub>28</sub> $\beta\alpha$ (S+R)-dia+ C <sub>27</sub> $\beta\alpha$ (S+R)-dia)
Q1	46.18	4.45	49.37	0.19	1.13
Q2	46.44	3.97	49.59	0.17	1.22
Q3	44.65	8.87	46.48	0.19	0.75
Q4	44.23	10.21	45.56	0.13	0.77
Q8	47.00	5.15	47.85	0.13	0.60
Q9	46.13	4.00	49.87	0.15	0.33
Q10	32.08	34.25	33.67	0.17	0.25
Q11	35.28	24.35	40.37	0.12	0.88
Q18	35.00	27.29	37.71	0.17	0.81
Q19	33.50	31.50	35.00	0.17	0.66
Q20	35.90	24.10	40.00	0.19	0.90
Q21	34.34	26.80	38.86	0.13	1.18

Table 3.6: Gas chromatogram data of steranes and diasteranes of the Qahash Coal  
(calculated on  $m/z$  217)

Sample No.	C <sub>27</sub>	C <sub>28</sub>	C <sub>29</sub>	C <sub>29</sub> ( $\beta\beta/\beta\beta+\alpha\alpha$ )	C <sub>29</sub> $\beta\alpha$ (S+R)-dia/ (C <sub>28</sub> $\beta\alpha$ (S+R)-dia+ C <sub>27</sub> $\beta\alpha$ (S+R)-dia)
Q5	20.05	11.45	68.50	0.20	1.36
Q6	18.63	14.20	67.17	0.20	1.95
Q7	21.20	8.87	69.93	0.19	1.23
Q12	20.79	10.21	69.00	0.22	1.55
Q13	22.73	4.45	72.82	0.21	1.15
Q14	23.00	3.90	73.10	0.21	1.29
Q15	21.83	14.05	64.12	0.20	1.52
Q16	21.55	17.09	61.36	0.19	1.10
Q17	19.19	12.91	67.90	0.19	1.33

Table 3.7: Gas chromatogram data of terpanes, hopanes and TPP ratios of the Qahash Shale (calculated on  $m/z$  217)

Sample No.	$C_{31}R/C_{30}H$	$C_{32} 22S/(22S+22R)$	$G/C_{30}$	Hopanes/ (Hopanes+ $\Sigma 20R$ steranes)	TPP ratios
Q1	0.52	0.44	0.75	0.51	0.21
Q2	0.49	0.40	0.80	0.50	0.18
Q3	0.48	0.39	0.56	0.47	0.24
Q4	0.48	0.36	0.66	0.54	0.16
Q8	0.50	0.36	0.71	0.36	0.17
Q9	0.50	0.39	0.80	0.41	0.16
Q10	0.47	0.39	0.83	0.33	0.18
Q11	0.53	0.39	0.53	0.31	0.22
Q18	0.55	0.37	0.55	0.37	0.18
Q19	0.55	0.41	0.89	0.49	0.19
Q20	0.50	0.42	0.91	0.55	0.23
Q21	0.47	0.42	0.77	0.51	0.21

Table 3.8: Gas chromatogram data of terpanes, hopanes and TPP ratios of the Qahash Coal (calculated on  $m/z$  217)

Sample No.	$C_{31}R/C_{30}H$	$C_{32} 22S/(22S+22R)$	$G/C_{30}$	Hopanes/ (Hopanes+ $\Sigma 20R$ steranes)	TPP ratios
Q5	0.46	0.33	0.91	0.64	0.22
Q6	0.44	0.33	0.93	0.60	0.17
Q7	0.47	0.35	0.83	0.49	0.21
Q12	0.46	0.37	0.91	0.67	0.25
Q13	0.46	0.37	0.74	0.58	0.19
Q14	0.45	0.33	0.70	0.33	0.20
Q15	0.48	0.32	0.84	0.51	0.20
Q16	0.47	0.36	0.93	0.55	0.23
Q17	0.46	0.36	0.79	0.63	0.16



Where:

TOC = Total organic carbon (wt. %).

$S_1$  = Amount of free hydrocarbons in sample (mg / g).

$S_2$  = Amount of hydrocarbons generated through thermal cracking (mg / g) – provides the quantity of hydrocarbons that the rock has the potential to produce through diagenesis.

$S_3$  = Amount of  $CO_2$  (mg of  $CO_2$  / g of rock) - reflects the amount of oxygen in the oxidation step.

$T_{max}$  = The temperature at which maximum rate of generation of hydrocarbons occurs.

Hydrogen index:  $HI = 100 * S_2 / TOC$ .

Oxygen index:  $OI = 100 * S_3 / TOC$ .

Production index:  $PI = S_1 / (S_1 + S_2)$ .

Semi-quantitative index:  $GP = S_1 / S_2$ .

Ro = Vitrinite reflectance (wt. %).

Pr / Ph = Pristane / Phytane.

Carbon preference index:  $CPI = 2(C_{23} + C_{25} + C_{27} + C_{29}) / (C_{22} + 2[C_{24} + C_{26} + C_{28}] + C_{30})$ .

Waxiness index:  $WI = \Sigma(n-C_{21}-n-C_{31}) / \Sigma(n-C_{15}-n-C_{20})$ .

TPP = Tetracyclic polyprenoid.

### 3.2. Statistical Treatment

The statistical treatment of the obtained data involves descriptive statistics (Table 3.9), correlation matrix (Table 3.10 and Fig. 3.1) and principal component analysis (PCA, Table 3.11 and Fig. 3.2) using the SPSS© program. The correlation matrix indicates that the analyzed parameters are mutually correlated (except for OI). These relations suggest the following:

- 1) The contribution of  $S_1$  and  $S_2$  from TOC.
- 2) The maturity of the studied source rocks is dependent of the amount of organic matter.
- 3) The immaturity of the organic matter.

There are three principal components (PCs). The components described 94.73 % of total variance of data. The following is a brief discussion of these components.

**First principal component (PC1):** It accounts for about 85.96 % of the total variables. It shows positive loading for TOC,  $T_{max}$ , Ro,  $S_1$ ,  $S_2$ ,  $S_3$ , HI and PI and negative loading for OI. It is the strongest component and is therefore important in interpreting organic matter richness, thermal maturation and organic matter type.

**Second principal component (PC2) and Third principal component (PC3):** They account for 6.22 and 2.55 % of the total variables, respectively. These components show no loading for any of the analyzed parameters and therefore have no significance.

*Table 3.9: Descriptive statistics of organic parameters of the studied shales and coals*

Parameters	N	Minimum	Maximum	Mean	Std. Deviation
TOC	21	0.22	0.88	0.55	0.24
$T_{max}$	21	411	423	416.48	3.92
Ro	21	0.23	0.52	0.38	0.10
$S_1$	21	0.12	4.07	2.00	1.62
$S_2$	21	0.17	2.43	1.28	0.96
$S_3$	21	0.49	1.18	0.86	0.22
HI	21	56.76	369.35	193.21	111.66
OI	21	109.76	234.48	173.97	45.56
PI	21	0.41	0.66	0.57	0.07

*Table 3.10: Correlation matrix of organic parameters of the studied shales and coals*

Parameters	TOC	$T_{max}$	Ro	$S_1$	$S_2$	$S_3$	HI	OI	PI
TOC	1.00								
$T_{max}$	0.79	1.00							
Ro	0.85	0.80	1.00						
$S_1$	0.96	0.81	0.89	1.00					
$S_2$	0.95	0.85	0.93	0.98	1.00				
$S_3$	0.86	0.82	0.86	0.83	0.90	1.00			
HI	0.86	0.84	0.92	0.94	0.98	0.89	1.00		
OI	-0.96	-0.69	-0.75	-0.92	-0.88	-0.71	-0.78	1.00	
PI	0.82	0.63	0.71	0.85	0.80	0.66	0.74	-0.81	1.00

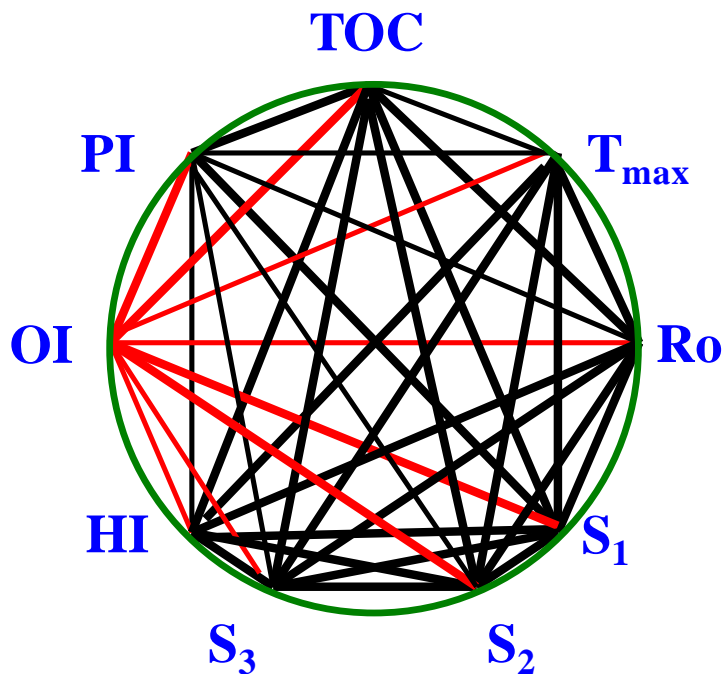


Fig. 3.1: Correlations among the analyzed organic parameters in the studied samples (intensity of lines corresponds to the strength of the correlation coefficient (< 0.4 to > 0.8) (red line means inverse relation).

Table 3.11: Rotated component matrix for data of organic parameters of the studied samples

Eigenvalues	7.74	0.56	0.23
% of Variance	85.96	6.22	2.55
Cumulative %	85.96	92.18	94.73
Principal components	PC1	PC2	PC3
TOC	0.97	-0.14	-0.18
T <sub>max</sub>	0.87	0.31	-0.02
Ro	0.93	0.19	0.10
S <sub>1</sub>	0.98	-0.11	-0.01
S <sub>2</sub>	0.99	0.04	-0.01
S <sub>3</sub>	0.90	0.28	-0.02
HI	0.95	0.17	0.09
OI	-0.90	0.34	0.26
PI	0.84	-0.41	0.33

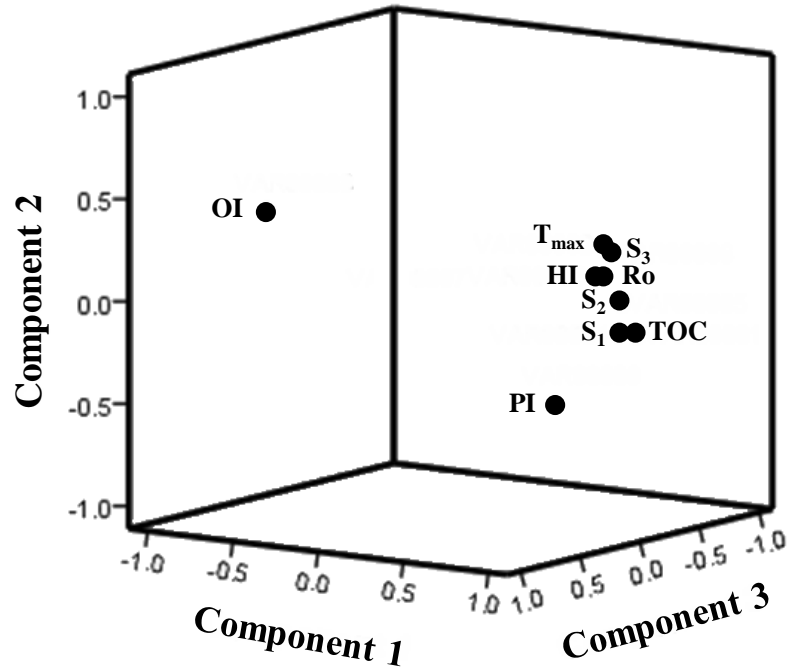


Fig. 3.2: Plot of PC loadings of the analyzed parameters.

### 3.3. Organic Matter Richness

The TOC is expressed as the relative dry weight percentage of organic carbon in the sediments (Mukhopadhyay *et al.*, 1997; Xia *et al.*, 2009; Godfray and Seetharamaiah, 2019), but not a direct measure of the total amount of organic matter (Alaug, 2013). It is generally accepted that for a rock to be a source of hydrocarbons, must contain sufficient organic matter for significant generation and expulsion for many years; this was taken as 0.5 % TOC for shales and somewhat less 0.3 % TOC for carbonates (Batten, 1996b). Peters and Cassa (1994) classified the organic richness into five grades: poor (TOC < 0.5 %), fair (0.5 % < TOC < 1%), good (1 % < TOC < 2 %), very good (2 % < TOC < 4 %) and excellent (TOC > 4 %). Furthermore, Ghorri (2002) and Dembicki (2009) designed models to assess source rock quality. These models are the plots of TOC vs. GP and TOC vs. S<sub>2</sub>. The shale samples have moderate TOC contents (> 0.5 %), whereas the coal samples contain lower values (< 0.5 %). Consequently, the Qahash Shale can be considered a fair source rock while the Qahash Coal has poor quality. The discrimination diagrams (Figs. 3.3-3.4) also supported this hypothesis.

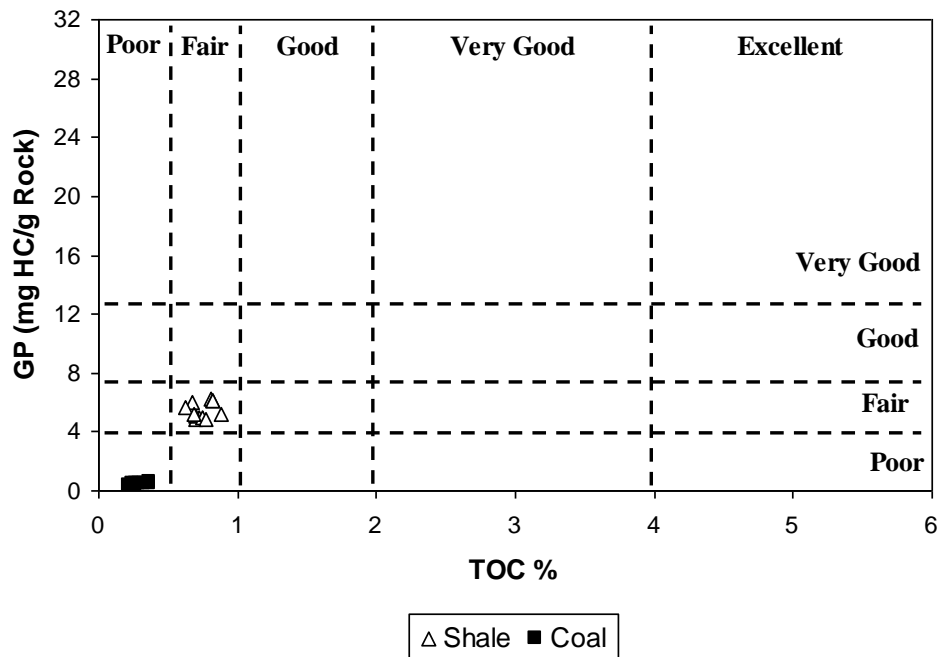


Fig. 3.3: Plot of TOC vs. GP showing the hydrocarbon potentialities for the studied samples (fields after Ghori, 2002).

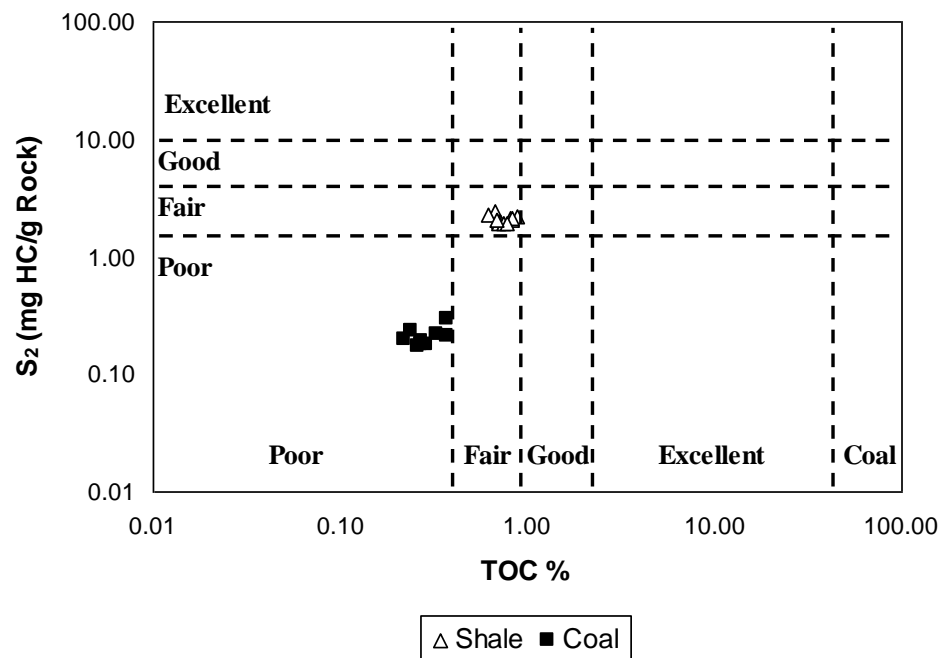


Fig. 3.4: Plot of TOC vs.  $S_2$  showing the hydrocarbon potentialities for the studied samples (fields after Dembicki, 2009).

### **3.4. Kerogen Classification and Thermal Maturity**

The portion of sedimentary organic matter which survived the initial decomposition process and is able to generate petroleum is called kerogen (Vandenbroucke, 2003). It is insoluble in organic solvents and represents the major organic carbon reservoir in the Earth's crust (Vandenbroucke, 2003). On the other hand, bitumen is the organic matter that is soluble in organic solvents. The elemental analysis of kerogen encompasses the following elements: C, H, N, O, S, and probable Fe from pyrite (Vandenbroucke and Largeau, 2007).

Biological activity at the early stage, following by temperature and pressure are responsible for the physiochemical transformation of organic matter in a sedimentary basin (Tissot and Welte, 1984). Higher temperatures and long period of geological time are involved in the transformation of kerogen into oil and gas (Ramos, 2015). Thus, increments in burial depth increase temperature and pressure, which along with geological time play an important role in the organic matter transformation (McCarthy *et al.*, 2011). It should be mentioned that the amount of hydrocarbons that might be generated in a source rock is exposed to kerogen composition and concentration, as well as the geothermal gradient evolution during burial history (Vandenbroucke, 2003).

The thermal maturation process, by which organic matter is altered changing its chemical composition and creating hydrocarbons, can be divided into three consecutively stages, diagenesis, catagenesis and metagenesis (Ramos, 2015). Diagenesis is the first stage of thermal maturation process of organic matter. It comprises the natural changes occurring from the moment of sediment depositions until the first signal of thermal alteration process (Ali *et al.*, 2010). Thus, this alteration starts in the water column (Vandenbroucke, 2003), being microbial activity the first process taking place (Tissot and Welte, 1984). The temperature, at which the alteration of organic matter in source rocks takes place, is ranged below 50° C (Vandenbroucke and Largeau, 2007). With reference to the depth interval, this phase is extended from one hundred to one thousand meters (Tissot and Welte, 1984). In this stage, oxidation along with other chemical process decomposes the material. On the one hand, anoxic deposition conditions might convert the material from biogenic gas into dry gas. The term biogenic gas is referred to the gas generated during the degradation of organic

matter in anaerobic conditions by bacterial microorganisms (Ramos, 2015). On the other hand, the increase of temperature and pH promote the transformation of organic matter into kerogen and bitumen.

Increasing burial depth due to successive sediment depositions, causes increment in pressure and temperature and the source rock undergoes catagenesis. During this phase, hydrocarbons are generated at temperatures range from 50 to 150°C and at several kilometers beneath the surface (Tissot and Welte, 1984). As a consequence, a thermal decomposition causes chemical bonds of kerogen breaks down, creating mostly oil but also gas (Peters *et al.*, 2005). A secondary cracking of oil molecules takes place during this phase due to the increment in temperature, generating wet gas such as methane, ethane, propane and heavier hydrocarbons (McCarthy *et al.*, 2011).

The last step in the thermal transformation of kerogen is called metagenesis. Temperature ranges from 150 to 200°C. In addition, to the higher burial depth might cause source rock be influenced by magma and hydrothermal effects (Tissot and Welte, 1984). Thus, at this stage, the increment in heat causes chemical changes within the kerogen, transforming it into methane and a carbon residue. Furthermore, late methane, or dry gas along with non-hydrocarbons gases such as CO<sub>2</sub>, N<sub>2</sub> and H<sub>2</sub>S might be generated as the source rock moves further down (McCarthy *et al.*, 2011).

Source rocks are said to be thermally immature, or potential source rocks, as the rocks have to be exposed to more heat in order to generate petroleum. Source rocks, which are found at the oil window, are said to be thermally mature or effective source rocks, as the rocks have been generating petroleum, or are actively generating it (Ramos, 2015). The last but not the least, source rocks are said to be thermally postmature, or spent source rocks, as the rocks have entered at the gas window and have already generated petroleum. Thus, they have consumed all the hydrogen necessary for further oil and gas generation (McCarthy *et al.*, 2011). On the other hand, it should be mentioned that maturation process can be also altered due to the influence of heat arising from the crustal tectonics or igneous bodies (Ramos, 2015).

In order to evaluate a source rock properly, a differentiation between kerogen types must be performed. As different types of organic matter have different chemical structures, the hydrocarbon potential varies (Tissot and Welte, 1984). Thus, four types of kerogen are distinguished based on its origin. Furthermore, the hydrogen, carbon and oxygen content can be used for such classification (Van Krevelen, 1961). Each type of kerogen can produce or generate different types of petroleum. In earlier times, kerogen classification used to be made based on its elemental composition. As soon as Rock-eval pyrolysis was developed, it was found that HI and OI parameters are directly proportional to H / C and O / C ratios, thus HI and OI replaced them on the Van Krevelen diagram, respectively (Mackenzie, 2005).

Type I kerogen originates mainly from lacustrine environments, although it can also be originated from marine environments. It is composed of algae, plankton and other matter which were reworked by bacteria and microorganisms. It shows high H / C atomic ratio and low O / C atomic ratio (Tissot and Welte, 1984). It is oil-prone, but depending on the thermal maturation phase can also generate gas. Type I kerogen is not usual and represents less than 3 % of oil and gas reserves in the world (Van Krevelen, 1961), although it presents high hydrocarbon potential (Tissot and Welte, 1984).

Type II kerogen originates in reducing environments from deep marine settings. Remains of plankton, among others, reworked by bacteria compose this kind of kerogen. It shows high H / C and low O / C ratios (Tissot and Welte, 1984). Type II kerogen can generate mainly oil, but also gas, providing enough heating and maturation (Vandenbroucke, 2003).

Type III kerogen derives from continental plants and contains vegetal debris. It has been deposited in shallow to deep marine or non-marine environments. It shows low initial H / C ratio and high initial O / C ratio (Tissot and Welte, 1984). This sort of kerogen usually generates dry gas (McCarthy *et al.*, 2011).

Type IV kerogen derives from residual organic matter which might have been altered by weathering, combustion or biologic oxidation in swamps or soils (McCarthy *et al.*, 2011).



It shows very low H / C ratio and a relatively high O / C ratio. This kind of kerogen is referred as a dead carbon, having no potential for petroleum generation (Tissot and Welte, 1984).

Equally important is the degree of hydrogen content in kerogens. Hydrogen-rich kerogens generate both oil and gas, nevertheless, hydrogen-poor kerogens generates mainly gas. Additionally, when hydrogen is depleted from kerogen, petroleum generation ceases, despite the amount of available carbon (Tissot and Welte, 1984).

To determine the type of kerogen and the degree of thermal maturity in the studied shales and coals, several parameters such as HI, OI, TOC, S<sub>1</sub>, S<sub>2</sub>, T<sub>max</sub> and Ro as well as the biomarker ratios were used. The plots of OI versus HI and TOC versus S<sub>2</sub> (Figs. 3.5-3.6) suggest that type II / III kerogen is dominant in the Qahash Shale, whereas the Qahash Coal is characterized by kerogens of type III and IV. Moreover, the plots of T<sub>max</sub> versus HI, T<sub>max</sub> versus Ro and C<sub>32</sub> 22S / (22S + 22R) homohopane versus C<sub>29</sub> (ββ / ββ + αα) sterane (Figs. 3.7-3.9) indicate that all organic matters are thermally immature. Additionally, the plot of TOC versus S<sub>1</sub> (Fig. 3.10) suggests that the Qahash Shale is characterized by nonindigenous (migrated) hydrocarbons, while the Qahash Coal contains indigenous (generated) hydrocarbons.

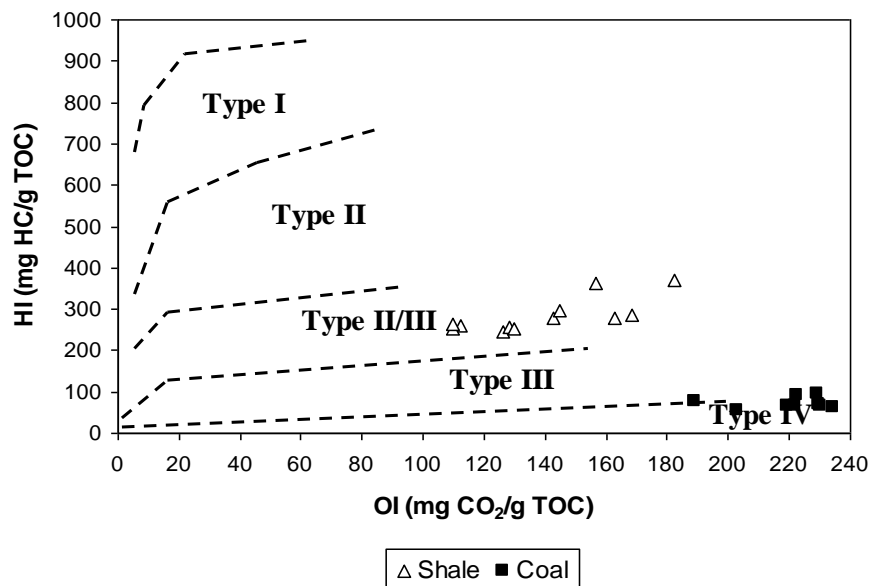


Fig. 3.5: Plot of OI vs. HI showing the kerogen type for the studied samples (fields after Van Krevelen, 1961).

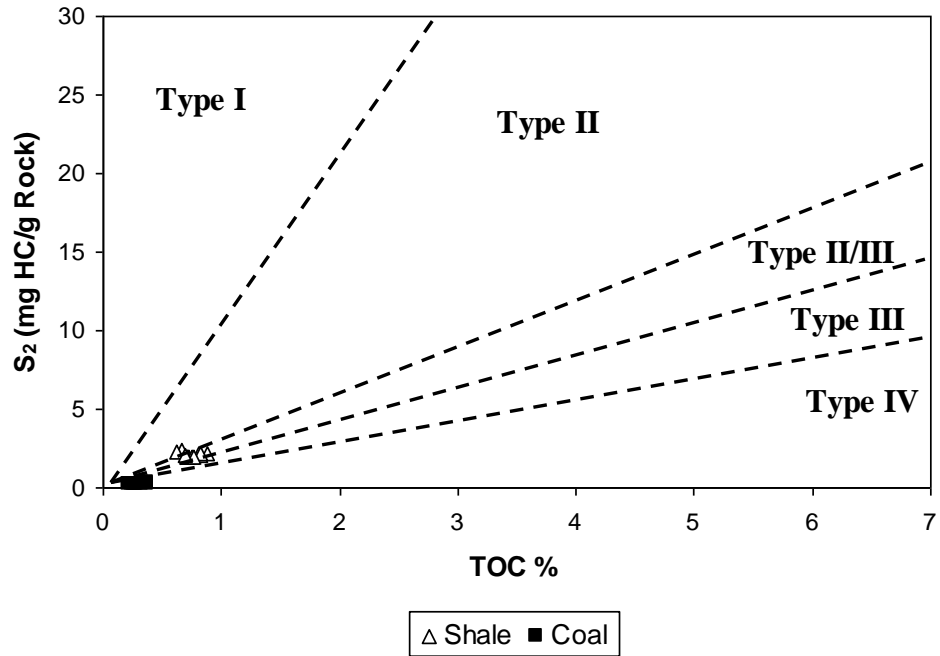


Fig. 3.6: Plot of TOC vs.  $S_2$  showing the kerogen type for the studied samples (fields after Longford and Blanc-Valleron, 1990).

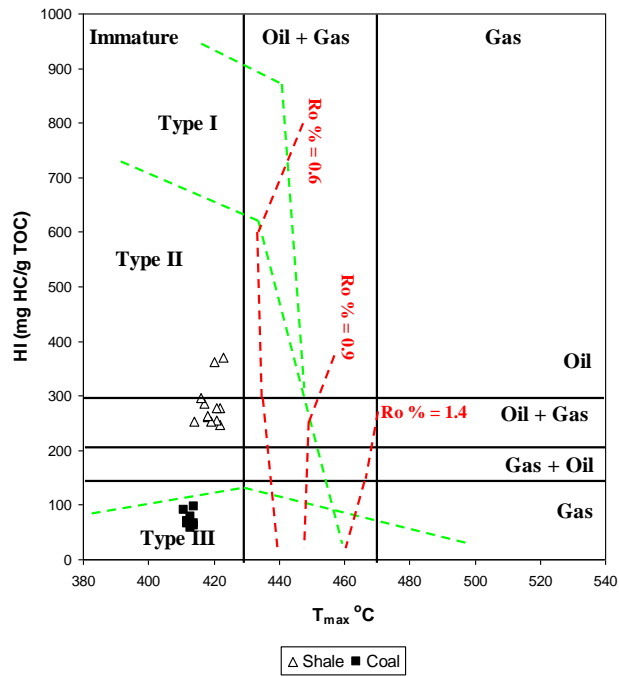


Fig. 3.7: Plot of  $T_{max}$  vs. HI showing the thermal maturity for the studied samples (fields after Hall et al., 2016).

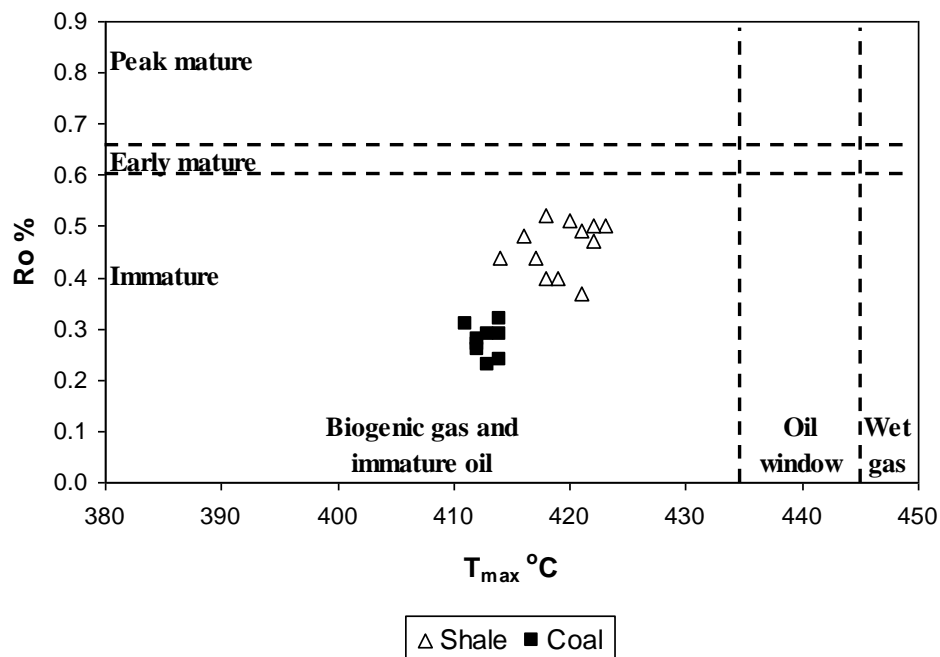


Fig. 3.8: Plot of  $T_{max}$  vs.  $Ro$  showing the thermal maturity for the studied samples (fields after Atta-Peters and Garrey, 2014).

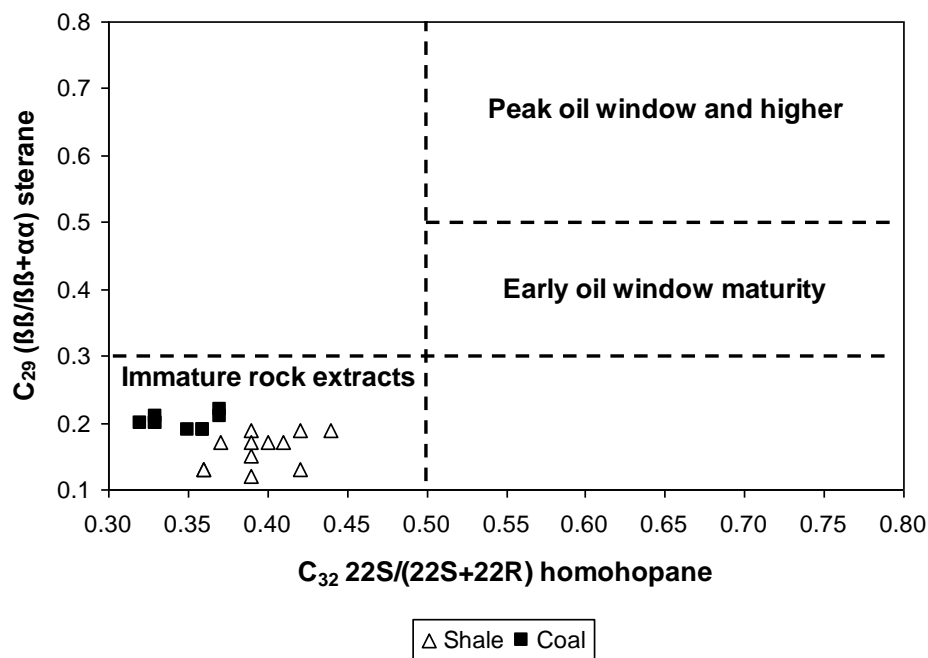


Fig. 3.9: Plot of  $C_{32} 22S / (22S + 22R)$  homohopane vs.  $C_{29} (\beta\beta / \beta\beta + \alpha\alpha)$  sterane showing the thermal maturity for the studied samples (fields after Peters and Moldowan, 1993).

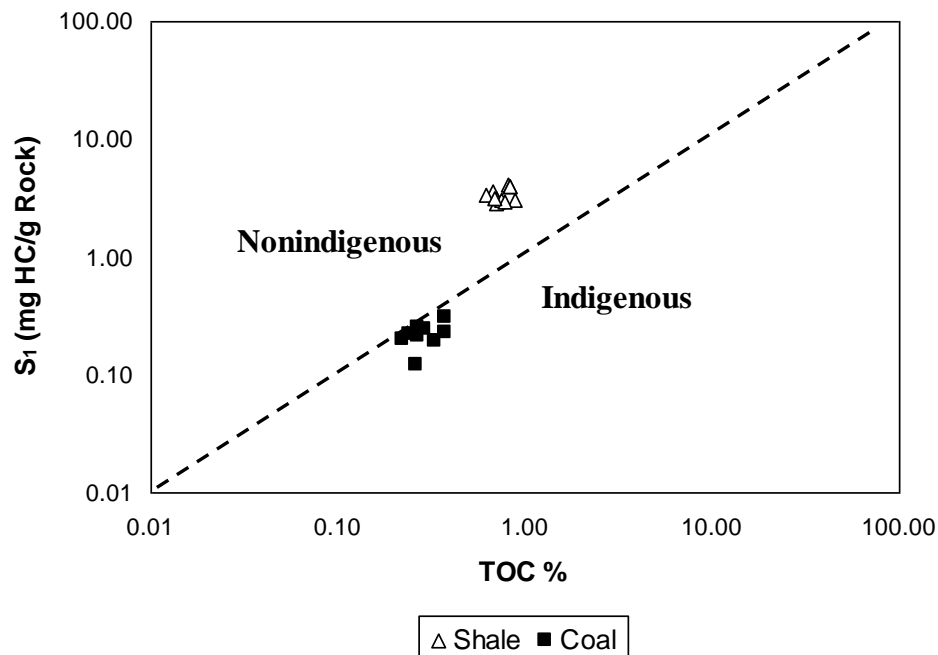


Fig. 3.10: Plot of TOC vs.  $S_1$  showing the status of hydrocarbons for the studied samples (fields after Hunt, 1996).

### 3.5. Organic Matter Input, Redox Conditions & Depositional Environment

Biological markers or biomarkers are molecular fossils, (originated from formerly living organisms), and are complex organic compounds composed of carbon, hydrogen, and other elements. They occur in sediments, rocks, and crude oils and show little or no change in structure from their parent organic molecules in living organisms (Peters *et al.*, 2005) and their carbon skeletons can be traced back to living organisms (Hunt, 1996).

The quality of information provided by the biomarkers or geochemical fossils in terms of depositional environment depends on three factors (Tissot and Welte, 1984):

- 1) Their state of conservation, which may or may not allow one to link them to their biochemical precursor molecule.
- 2) The distribution of the biochemical precursor (parent molecule) in the present animal and / or plant kingdom.
- 3) The assumption that the distribution was comparable in ancient organisms.

The utility of biomarkers as indicators of depositional environments arises from the fact that certain types of compounds are associated with organisms or plants that grow in specific types of depositional environments (Tissot and Welte, 1984).

Broocks *et al.*, (1969) noted the presence of the regular isoprenoids pristane (Pr) and phytane (Ph) in crude oils and coal extracts. This led Didyk *et al.*, (1978) to propose a mechanism for the production of relatively high concentrations of pristane in oxic type environments and high concentration of phytane in reducing type environments. Thus, the Pr / Ph ratio evolved as an indicator of the oxicity of the depositional environment.

Because some biomarkers pointed to specific taxa, they can also act as indicators of specific habitats. Fresh water environments are often indicated by the presence of biomarkers of typical fresh water organisms such as *Botryococcus braunii*. Lacustrine conditions are often indicated by the predominance of algal steroids (Tissot and Welte, 1984). Hypersaline lakes and ponds often develop anoxic conditions if saline deep water is covered with water of lower density. Sedimentary rocks that were deposited under these conditions often contain high relative concentrations of gammacerane, which is a biomarker generally associated with water column stratification (Tissot and Welte, 1984).

Rearranged steranes (diasteranes) are relatively more abundant in clastic sediments than in carbonates (Peters *et al.*, 2005). Hopanoide appear to be similarly affected so that diahopanes and neohopanes are relatively more prominent in bitumen and oils derived from shales as opposed carbonates (Peters and Moldowan, 1993). However increase in thermal maturity is also a key factor in the conversion of biomarkers to their rearranged forms.

In this study, details of biomarker characteristics have been examined based on the distributions of normal alkanes, isoprenoids, steranes diasteranes, terpanes and hopanes. The plots of Pr / Ph versus  $C_{31}22R / C_{30}$ - Hopane, Pr / Ph versus  $(Pr + n-C_{17}) / (Ph + n-C_{18})$  and Hopanes /  $(Hopanes + \sum 20R \text{ steranes})$  versus TPP (Figs. 3.11-3.13) suggest that the marine environment is the proved origin of the Qahash Formation. Furthermore, the biplots of Pr / Ph versus WI, Pr / Ph versus CPI, Pr / Ph versus  $C_{29} / C_{27}$  regular steranes, Pr / Ph versus

$\sum(n-C_{12}-n-C_{20}) / (\sum(n-C_{12}-n-C_{20}) + \sum(n-C_{12}-n-C_{29}))$ , Pr / Ph versus  $C_{29} \beta\alpha(S + R)\text{-dia} / (C_{28} \beta\alpha(S + R)\text{-dia} + C_{27} \beta\alpha(S + R)\text{-dia})$  and Ph / n-C<sub>18</sub> versus Pr / n-C<sub>17</sub> (Figs. 3.14-3.19), and the triplot of C<sub>27</sub>-C<sub>28</sub>-C<sub>29</sub> regular steranes (Fig. 3.20) indicate that the Qahash Shale contains mixed organic matter formed in suboxic conditions, while the Qahash Coal is characterized by terrigenous organic matter formed in oxic conditions. In addition, the plot of Pr / Ph versus G / C<sub>30</sub> (Fig. 3.21) refers to deposition in high saline water.

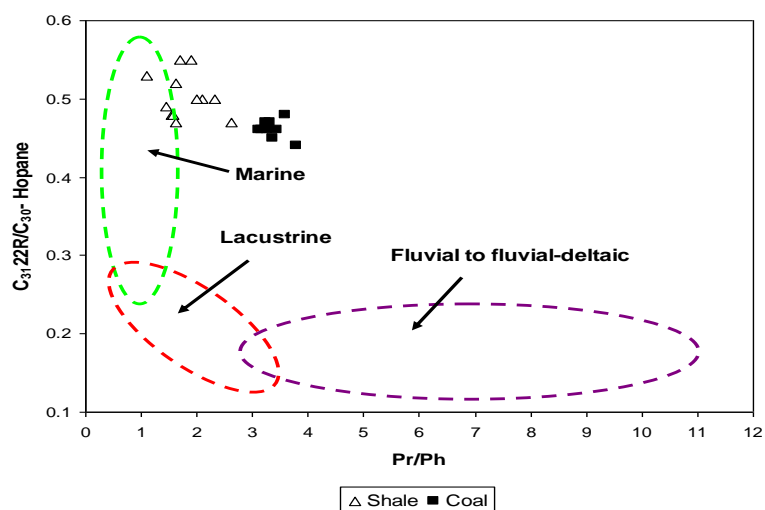


Fig. 3.11: Plot of Pr / Ph vs. C<sub>31</sub>R / C<sub>30</sub> hopane showing the depositional environment of the Qahash Formation (fields after Peters et al., 2005).

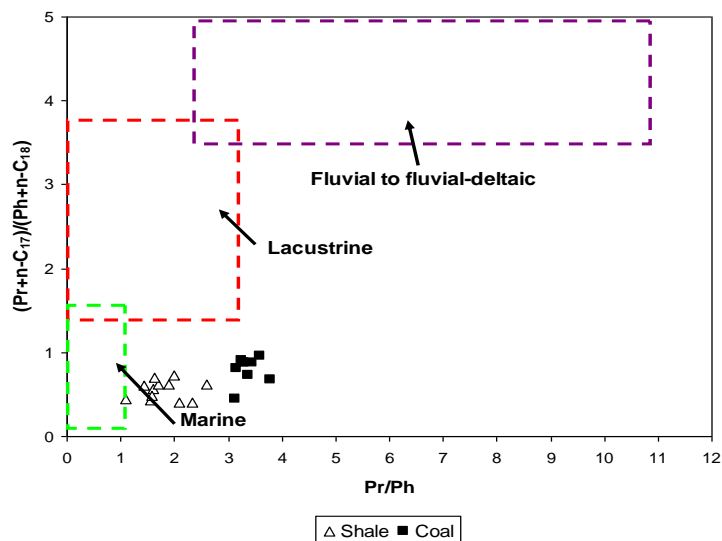


Fig. 3.12: Plot of Pr / Ph vs. (Pr + n-C<sub>17</sub>) / (Ph + n-C<sub>18</sub>) showing the depositional environment of the Qahash Formation (fields after Shaltami et al., 2019).

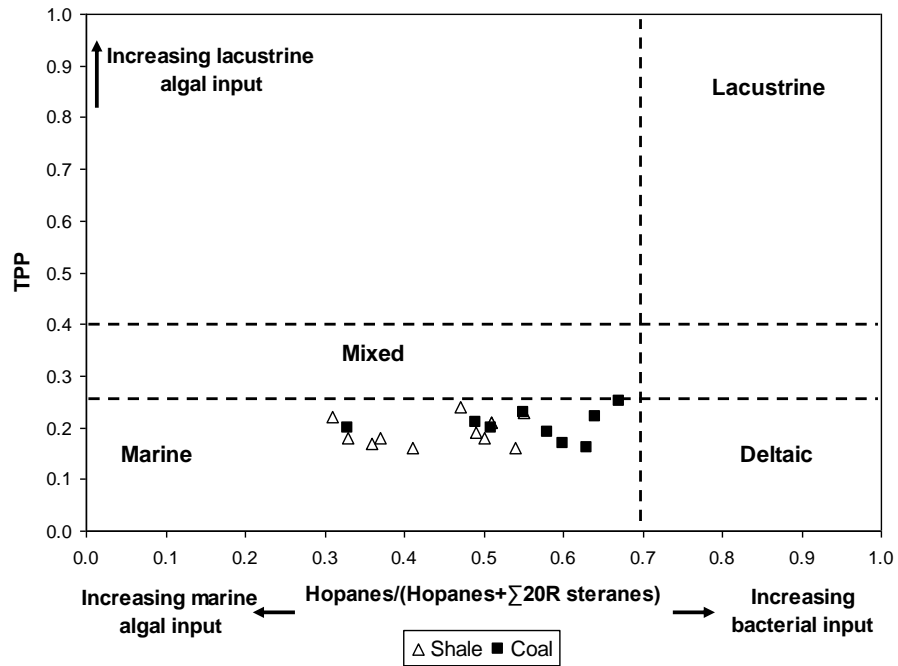


Fig. 3.13: Plot of TPP vs. hopane / (hopanes +  $\Sigma 20R$  steranes) showing the depositional environment of the Qahash Formation (fields after Holba et al., 2003).

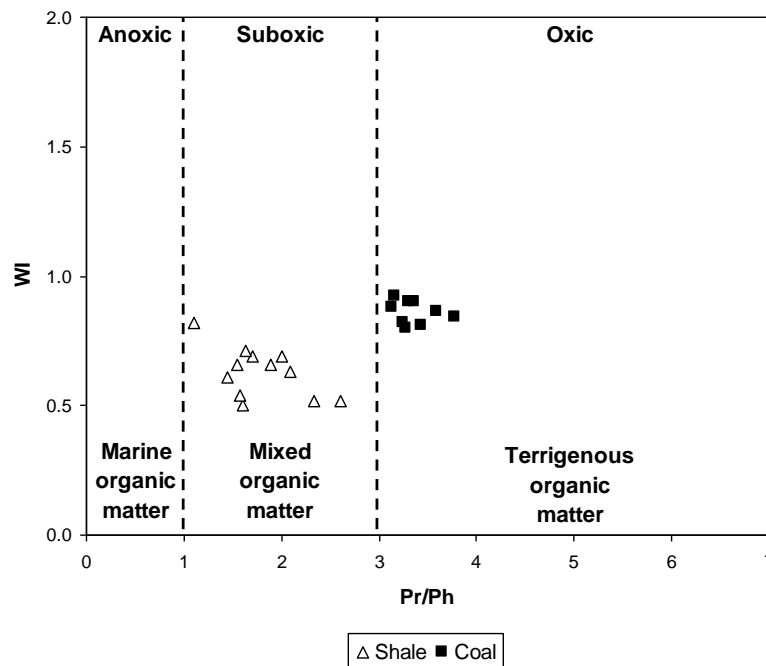


Fig. 3.14: Plot of Pr / Ph vs. WI showing the organic matter origin and redox conditions for the studied samples (fields after El Diasty and Moldowan, 2012).

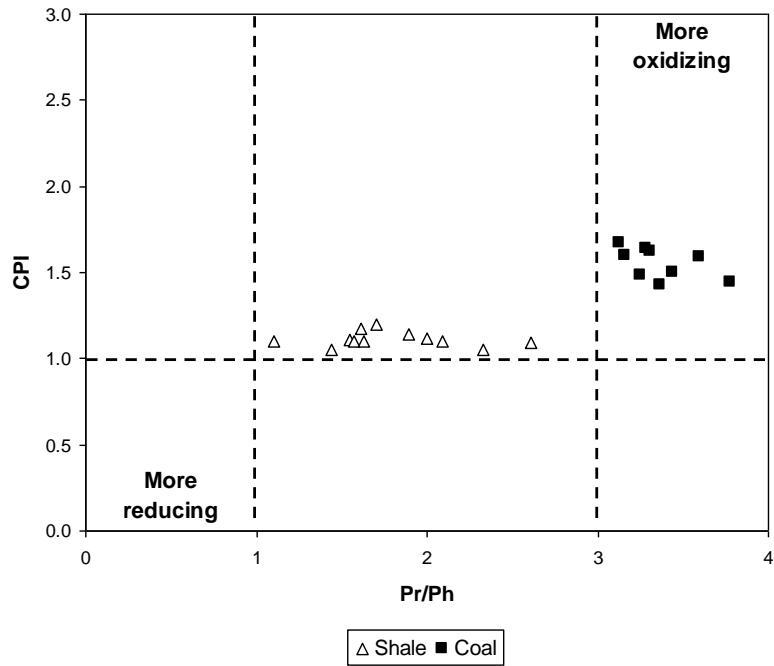


Fig. 3.15: Plot of Pr / Ph vs. CPI showing the organic matter origin and redox conditions for the samples (fields after Akinlua et al., 2007).

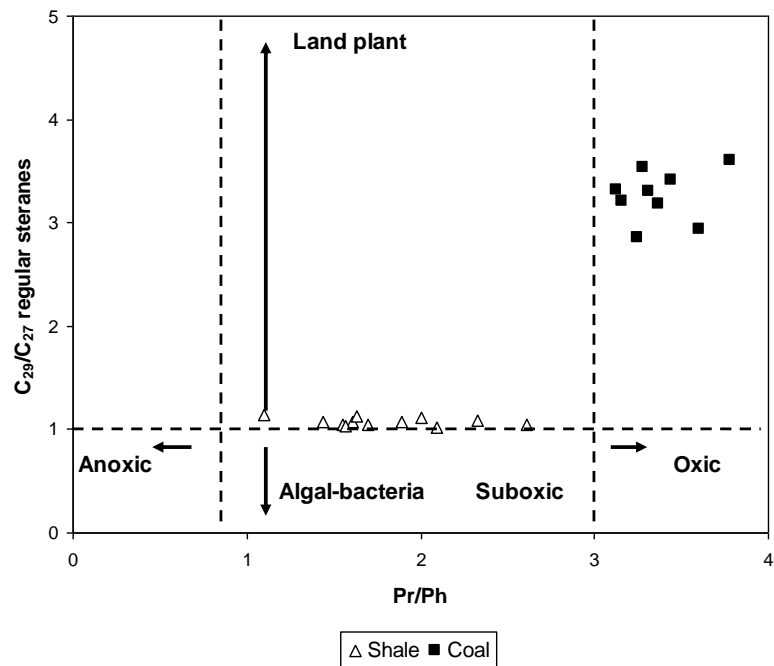


Fig. 3.16: Plot of Pr / Ph vs. C<sub>29</sub> / C<sub>27</sub> regular steranes showing the organic matter origin and redox conditions for the studied samples (fields after Yandoka et al., 2015).



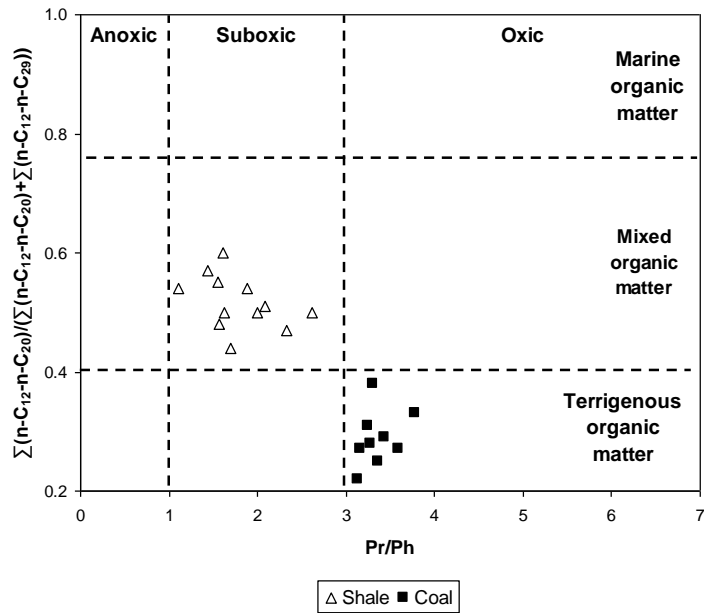


Fig. 3.17: Plot of  $Pr / Ph$  vs.  $n$ -alkane SLR ( $\sum n-C_{12-20} / \sum n-C_{12-29}$ ) showing the organic matter origin and redox conditions for the studied samples (fields after Shaltami et al., 2019).

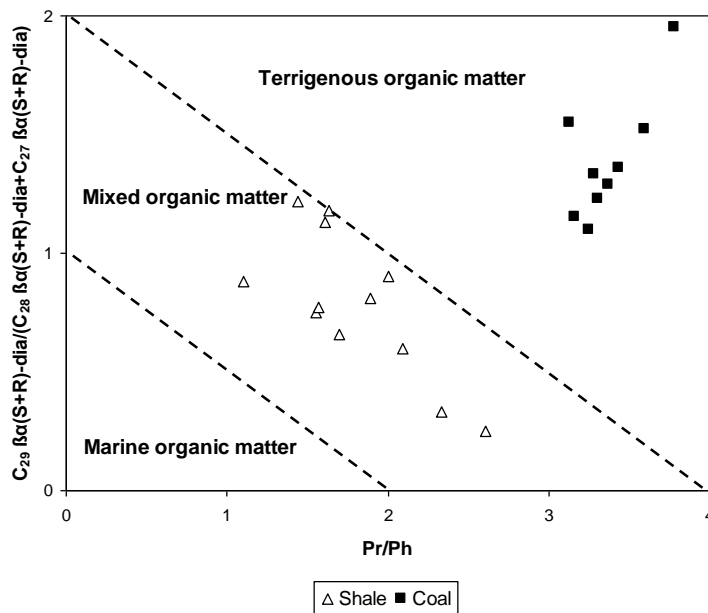


Fig. 3.18: Plot of  $Pr / Ph$  vs. predominance of  $C_{29}$ -components amongst diasteranes showing the organic matter origin for the studied samples (fields after Shaltami et al., 2019).

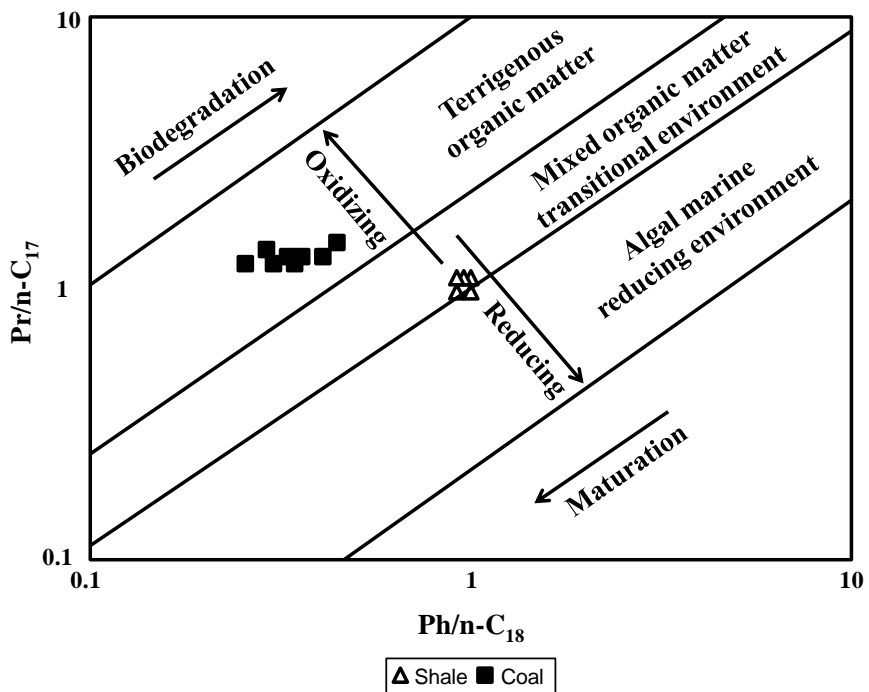


Fig. 3.19: Plot of  $Ph / n-C_{18}$  vs.  $Pr / n-C_{17}$  showing the organic matter origin and redox conditions for the studied samples (fields after Shanmugam, 1985).

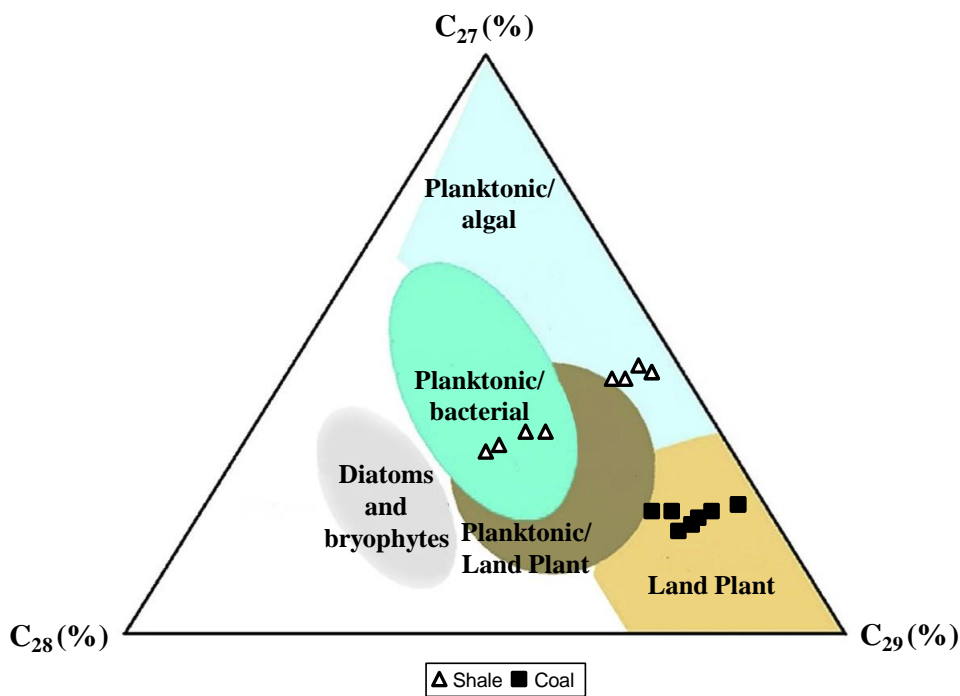


Fig. 3.20: Ternary diagram of  $C_{27}$ - $C_{28}$ - $C_{29}$  regular steranes showing the organic matter origin for the studied samples (fields after Huang and Meinschein, 1979).

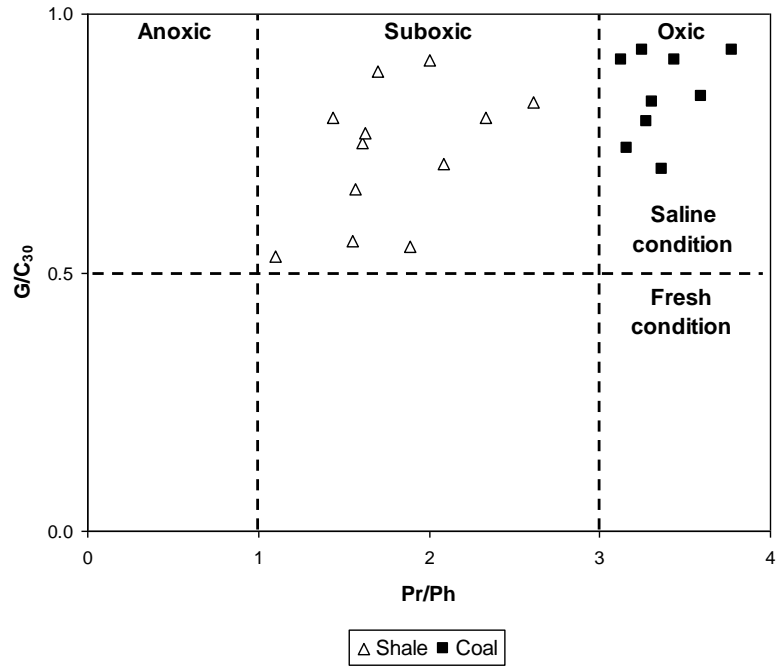


Fig. 3.21: Plot of  $Pr / Ph$  vs.  $G / C_{30}$  showing the paleosalinity and redox conditions for the studied samples (fields after Zhou and Huang, 2008).

**CHAPTER FOUR**  
**CONCLUSIONS**

## **CHAPTER FOUR**

### **CONCLUSIONS**

According to the results which recorded in this study, the shales and coals of the Qahash Formation were evaluated in the offshore well AI-NC 128. Summarizing, this work aims to assess the quality of the source rocks, characterize the type of organic matter, as well as determining its maturity status in order to deduce the hydrocarbon potential, using organic petrography, scanning electron microscope, Rock-Eval pyrolysis and gas chromatography-mass spectrometry. The following are the main conclusions of the current study:

- 1) The detected macerals are Vitrinite (ulminite, textinite, collotelinite, telinite, densinite, attrinite, corpohuminite and gelinite), Liptinite (sporinite, cutinite, alginite, resinite, subernite and bituminite) and Inertinite (fusinite, semifusinite, inertodetrinite, funginite, macrinite and micrinite).
- 2) The mineral matter is mainly represented by framboidal pyrite.
- 3) The macerals and biomarkers suggest the domination of humid conditions with high salinity during the deposition of the Qahash Formation.
- 4) Generally, the shales and coals were deposited in a limno-telmatic condition.
- 5) The Qahash Shale is a fair source rock, while the Qahash Coal has a poor quality.
- 6) The Qahash Shale behaves as type II / III kerogen, whereas the Qahash Coal is characterized by kerogens of type III and IV.
- 7) All organic matters are thermally immature.
- 8) The Qahash Shale is characterized by mixed organic matter formed in suboxic to anoxic conditions, while the Qahash Coal contains terrigenous organic matter formed in oxidizing conditions.

## **REFERENCES**

## References

**Akinlua, A., Ajayi, T.R. and Adeleke, B.B. (2007):** Organic and inorganic geochemistry of northwestern Niger Delta oils. *Geochemical Journal*; 41: 271-281.

**Alaug, A.S., Batten, D.J. and Ahmed, A.F. (2013):** Organic geochemistry, palynofacies and petroleum potential of the Mukalla formation (Late Cretaceous), Block 16, eastern Yemen. *Marine and Petroleum Geology*; 46: 67-91.

**Ali, S., Clark, W.J., Moore, W.R., and Dribus, J.R. (2010):** Diagenesis and reservoir quality. *Oilfield Review*; 22(2): 14-27.

**Amijaya, H. and Littke, R. (2005):** Microfacies and depositional environment of Tertiary Tanjung Enim low rank coal, South Sumatra Basin, Indonesia. *International Journal of Coal Geology*; 61: 197-221.

**Atta-Peters, D. and Garrey, P. (2014):** Source rock evaluation and hydrocarbon potential in the Tano basin, South Western Ghana, West Africa. *International Journal of Oil, Gas and Coal Engineering*; 2(5): 66-77.

**Asahina, K. and Suzuki, N. (2019):** Methylated naphthalenes as indicators for evaluating the source and source rock lithology of degraded oils. *Organic Geochemistry*; 124: 46-62.

**Batten D.J. (1996b):** Palynofacies and petroleum potential. In: Jansonius J, McGregor DC (eds) *Palynology: principles and applications*, vol 3. American Association of Stratigraphic Palynologists Foundation, Dallas; pp. 1065-1084.

**Brooks, J.D., Gould, K. and Smith, J.W. (1969):** Isoprenoid hydrocarbons in coal and petroleum. *Nature*; 222: 257-259.

**Buitrago, J., Diaz, C., Gruenwald, R., Suarez, J. and Tawengi, K.S. (2011):** New insights into the stratigraphy and petroleum geology of western Cyrenaica, NE Libya. 5<sup>th</sup> North African Mediterranean Petroleum and Geosciences Conference and Exhibition, Tripoli, Libya.

**Calder, J.H., Gibbing, M.R. and Mukhopadhyay, P.K. (1991):** Peat formation in a Westphalian B piedmont setting, Cumberland Basin, Nova Scotia: Implication for the maceral based interpretation of reotrophic and raised paleomires. *Bulletin de la Société Géologique de France*; 162: 283-298.

**Carmignani, L. (1984):** Geological map of Libya, 1:250000, Sheet: Wadi Al Hamim, NH 34-7, Explanatory Booklet, Industrial Research Center (IRC), Tripoli, 98p.

**Carvajal-Ortiz, H. and Gentzis, T. (2015):** Critical considerations when assessing hydrocarbon plays using Rock-Eval pyrolysis and organic petrology data: Data quality revisited. *International Journal of Coal Geology*; 152(A): 113-122.

**Crosdale, P.J. (1993):** Coal maceral ratios as indicators of environment of deposition: do they work for ombrogenous mires? An example from the Miocene of New Zealand. *Organic Geochemistry*; 20: 797-809.

**Dembicki, H.J. (2009):** Three common source rock evaluation errors made by geologists during prospect or play appraisals. *AAPG Bulletin*; 93(3): 341-356.

**Di Cesare, F., Franchino, A. and Sommaruga, C. (1963):** The Pliocene-Quaternary of Giarabub Erg region. *Rev. l'Inst. Fr. Petrol.*; 18(10): 1344-1362.

**Diessel, C.F.K. (1986):** On the correlation between coal facies and depositional environments. *Proc. 20th Newcastle Symp. The University of Newcastle*; pp. 19-22.



**Diessel, C.F.K. (1992):** The problem of syn-versus post depositional marine influence on coal composition. In: Proceedings of the advances in the study of the Sydney Basin, 26th Newcastle Symposium; pp. 154-163.

**Didyk, B.M., Simoneit, B.R.T., Brassell, S.C. and Eglinton, G. (1978):** Organic geochemical indicators of paleoenvironmental conditions of sedimentation. *Nature*; 272: 216-222.

**Duronio, P., Dakshe, A. and Bellini, E. (1991):** Stratigraphy of the offshore Cyrenaica (Libya). Third Symposium on the Geology of Libya, vol. 4 (eds. M.J. Salem, O.S. Hammuda and B.A. Eliagoubi), Elsevier, Amsterdam, pp. 1589-1620.

**El Diasty, W.S. and Moldowan, J.M. (2012):** Application of biological markers in the recognition of the geochemical characteristics of some crude oils from Abu Gharadig Basin, north Western Desert–Egypt. *Marine and Petroleum Geology*; 35:28-40.

**El Hawat, A.S. and Abdulsamad, E.O. (2004):** The Geology of Cyrenaica: A Field Seminar. *Geology of East Libya, Field Trip, ESSL, Tripoli, Libya*, 130 p.

**El Hawat, A.S. and Shelmani, M.A. (1993):** Short notes and guidebook on the geology of Al Jabal Al Akhdar, Cyrenaica, NE Libya. Interprint Limited Malta, 70p.

**El-Khadragy, A.A., Shazly, T.F., Mousa, D.A., Ramadan, M. and El-Sawy, M.Z. (2019):** Integration of well log analysis data with geochemical data to evaluate possible source rock. Case study from GM-ALEF-1 well, Ras Ghara oil Field, Gulf of Suez-Egypt. *Egyptian Journal of Petroleum*; 27(4): 911-918.

**Francis, M. and Issawi, B. (1977):** Geological Map of Libya, 1:250000, Sheet: Soluq, NI 34-2, Explanatory Booklet, Industrial Research Center (IRC), Tripoli, 86p.

**Flores, D. (2002):** Organic facies and depositional palaeoenvironment of lignites from Rio Major Basin (Portugal). *International Journal of Coal Geology*; 48: 181-195.

**Garming, J. F. L.; Bleil, U. and Riedinger, N. (2005):** Alteration of magnetic mineralogy at the sulfate–methane transition: Analysis of sediments from the Argentine continental slope. *Physics of the Earth and Planetary Interiors*; 151(3-4): 290-308.

**Ghori, K.A.R. (2002):** Modeling the hydrocarbon generative history of the Officer Basin, Western Australia. *Journal of Philosophy of Education Society of Australasia (PESA)*; 29: 29-42.

**Giammarino, S. (1984):** Geological Map of Libya, 1:250000, Sheet: Wadi Al Khali, NI 34-8, Explanatory Booklet, Industrial Research Center (IRC), Tripoli, 73p.

**Godfray, G. and Seetharamaiah, J. (2019):** Geochemical and well logs evaluation of the Triassic source rocks of the Mandawa basin, SE Tanzania: Implication on richness and hydrocarbon generation potential. *Journal of African Earth Sciences*; 153: 9-16.

**Hakimi, M.H., Abdullah, W.H. and Shalaby, M.R. (2010):** Source rock characterization and oil generating potential of the Jurassic Madbi Formation, onshore East Shabawah oilfields, Republic of Yemen. *Organic Geochemistry*; 41(5): 513-521.

**Hall, L.S., Boreham, C.J., Edwards, D.S., Palu, T.J., Buckler, T., Hill, A.J. and Troup, A. (2016):** Cooper Basin source rock geochemistry: Regional hydrocarbon prospectivity of the Cooper Basin. *Geoscience Australia, Part2*; 62p.

**Hallett, D. (2002):** Petroleum geology of Libya. Amsterdam, Elsevier Inc., 503p.

**Hallett, D. and Clark-Lowes, D. (2016):** Petroleum geology of Libya. 2<sup>nd</sup> edition, Amsterdam, Elsevier Inc., 404p.

**He, C., Ji, L., Su, A., Wu, Y., Zhang, M., Zhou, S., Li, J., Hao, L. and Ma, Y. (2019):** Source-rock evaluation and depositional environment of black shales in the Triassic

Yanchang Formation, southern Ordos Basin, north-central China. *Journal of Petroleum Science and Engineering*; 173: 899-911.

**Holba, A.G., Dzoub, L.I., Wood, G.D., Ellisd, L., Adame, P., Schaeffere, P., Albrechte, P., Greenef, T. and Hughes, W.B. (2003):** Application of tetracyclic polyprenoids as indicators of input from fresh-brackish water environments. *Organic Geochemistry*; 34: 441-469.

**Huang, W.Y. and Meinschein, W.G. (1979):** Sterols as ecological indicators. *Geochimica et Cosmochimica Acta*; 43: 739-745.

**Hunt, J.M. (1996):** *Petroleum geochemistry and geology*, 2<sup>nd</sup> edition, vol. 743. New York: Freeman and Company.

**ICCP System (1994a):** Methods for the petrographic analysis of bituminous coal and anthracite-part 3: method of determining maceral group composition-ISO 7404-33:1994. ISO, Geneva.

**ICCP System (1994b):** Methods for the petrographic analysis of bituminous coal and anthracite-part 5: method of determining Microscopically the reflectance of vitrinite-ISO 7404-53: 1994. ISO, Geneva.

**ISO 11760 (2005):** Classification of coals. International Standard; 9p.

**ISO 7404-2 (2009):** Methods for the petrographic analysis of bituminous coal and anthracite-part 2: Methods of preparing coal samples. International Organization for Standardization, ISO, Geneva; 8p.

**ISO 7404-3 (2009):** Methods for the petrographic analysis of bituminous coal and anthracite-part 3: Methods of determining maceral group composition. International Organization for Standardization, ISO, Geneva; 4p.

**ISO 7404-5 (2009):** Methods for the petrographic analysis of bituminous coal and anthracite-part 5: Methods of determining microscopically the reflectance of vitrinite. International Organization for Standardization ISO, Geneva; 11p.

**Kalaitzidis, S., Bouzinos, A. and Christanis, K. (2000):** Paleoenvironment of lignite formation prior to and after the deposition of the “characteristic sand” in the lignite deposit of Ptolemais. *Miner Wealth, Athens*; 115: 29-42.

**Klen, L. (1974):** Geological map of Libya, 1:250000, Sheet: Benghazi, NI 34-14, Explanatory Booklet, Industrial Research Center (IRC), Tripoli, 56p.

**Kruszewska, K.J. (2003):** Fluorescing macerals in South African coals. *International Journal of Coal Geology*; 54(1-2): 79-94.

**Lamberson M.N., Bustin R.m. and Kalkreuth, W. (1991):** Lithotype (maceral) composition and variation as correlated with paleo-wetland environments, Gates Formation, North eastern British Columbia, Canada. *International Journal of Coal Geology*; 18: 87-124.

**Longford, F.F. and Blanc-Valleron, M.M. (1990):** Interpreting Rock–Eval pyrolysis data using graphs of pyrolyzable hydrocarbons vs. total organic carbon, *AAPG Bulletin*; 74: 799-804.

**Mackenzie, F.T. (2005):** *Sediments, Diagenesis, and Sedimentary Rocks*. 1<sup>st</sup> edition, Elsevier Science, 446 p.

**Marshall, C.P., Kannangara, G.S.K., Wilson, M.A., Guerbois, J.P., Hartung-Kagi, B. and Hart, G. (2002):** Potential of thermogravimetric analysis coupled with mass spectrometry for the evaluation of kerogen in source rocks. *Chemical Geology*; 184(3-4): 185-194.

**Mazhar, A. and Issawi, B. (1977):** Geological Map of Libya, 1:250000, Sheet: Zt. Msus, NI 34-3, Explanatory Booklet, Industrial Research Center (IRC), Tripoli, 80p.

**McCarthy, K., Rojas, K., Niemann, M., Palmowski, D., Peters, K., and Stankiewicz, A. (2011):** Basic Petroleum Geochemistry for Source Rock Evaluation. *Oilfield Review*; 23(2): 32-43.

**Mijalkovic, N. (1977):** Geological Map of Libya, 1:250000, Sheet: Al Qaddahiyah, NH 33-3, Explanatory Booklet, Industrial Research Center (IRC), Tripoli, 66p.

**Moore, T.A. and Shearer, J.C. (2003):** Peat / coal type and depositional environment-are they related? *International Journal of Coal Geology*; 56: 233-252.

**Mukhopadhyay, P.K., Goodarzi, F., Kruge, M.A. and Alimi, M.H. (1997):** Comparison of source rock geochemistry of selected rocks from the Schei Point group and Ringnes formation, Sverdrup basin, arctic Canada. *International Journal of Coal Geology*; 34(3-4): 225-260.

**Ohfuji, H. and Rickard, D. (2005):** Experimental synthesis of framboids-a review. *Earth Science Reviews*; 71: 147-170.

**Palacas, J.G. (1988):** Characteristics of Carbonate Source Rocks of Petroleum. In *Petroleum Systems of the United States*, Washington, DC: US Geological Survey Bulletin; 1870: 20-25.

**Peters, K.E. and Cassa, M.R. (1994):** Applied source rock geochemistry. In: Magoon, L.B., Dow, W.G. (Eds.): *The petroleum system from source to trap*, AAPG, Mem.; 60: 93-117.

**Peters, K.E. and Moldowan, J.M. (1993):** *The biomarker guide: Interpreting molecular fossils in petroleum and ancient sediments*. Prentice-Hall, Inc, Englewood Cliffs, New Jersey.

**Peters, K.E., Walters, C.C. and Moldowan, J.M. (2005):** The biomarker guide: Biomarkers and isotopes in petroleum exploration and Earth history. 2<sup>nd</sup> edition, vol. 2. Cambridge University Press, Cambridge.

**Pietersz, C.R. (1968):** Proposed nomenclature for rock units in Northern Cyrenaica. In: Barr, F.T. (Ed.), Geology and Archaeology of Northern Cyrenaica, Libya. The Petroleum Exploration Society of Libya, 10th Annual Conference, Tripoli, pp. 125-130.

**Ramos, C.E.A. (2015):** Geochemical source rock evaluation in the Lusitanian Basin (Portugal) using TG/DSC analysis. Unpublished MSc Thesis, Tecnico Lisboa, Portugal.

**Rohlich, P. (1974):** Geological Map of Libya, 1:250,000, Sheet: Al Bayda, NI 34-15, Explanatory Booklet, Industrial Research Center (IRC), Tripoli, Libya, 70p.

**Rohlich, P. (1980):** Tectonic development of Al Jabal Al Akhdar in: Geology of Libya, Salem. M and Buserwil, London, Vol. III, pp. 923-931.

**Scott, A.C. (2002):** Coal petrology and the origin of coal macerals: a way ahead? International Journal of Coal Geology; 50: 119-134.

**Sengupta, S. (2013):** Coal geology and its application in industrial use. 1<sup>st</sup> edition. Srinivas Press, India.

**Shaltami, O.R. (2012):** Mineral composition and environmental geochemistry of the beach sediments along the Mediterranean Coast from Benghazi to Bin Jawwad, Northeast Libya. Unpublished PhD Thesis, Cairo University, Egypt.

**Shaltami, O.R., Fares, F.F., EL Oshebi, F.M., and Errishi, H. (2017):** Isotope age of the Early Oligocene shallow marine carbonates, Al Jabal Al Akhdar, NE Libya. The 12<sup>th</sup> International Symposium on Applied Isotope Geochemistry (AIG-12), Copper Mountain, Colorado, USA, Proceeding Book; pp. 23-34.

**Shaltami, O.R., Fares, F.F., EL Oshebi, F.M., Errishi, H. and Bustany, I. (2018):** High-resolution strontium isotope stratigraphy of the Eocene deposits in the Al Jabal Al Akhdar, NE Libya. 20<sup>th</sup> International Sedimentological Congress (ISC), Québec, Canada, Proceeding Book; pp. 33-42.

**Shaltami, O.R., Fares, F.F., EL Oshebi, F.M., Errishi, H. and Bustany, I. (2018):** Strontium isotopes as paleo-indicators of unconformities: A case of the Late Cretaceous-Paleocene deposits in the Al Jabal Al Akhdar, NE Libya. International Conference on Scientific Research and Innovation (ICSRI), Chennai, India, Proceeding Book; pp. 12-22.

**Shaltami, O.R., Fares, H., EL Oshebi, F.F., Errishi, F.M., Bustany, I. and Musa, M.M. (2018):** Depositional environment and absolute age of the Pliocene-early Pleistocene sediments in the Cyrenaica Basin, NE Libya. 16<sup>th</sup> Annual Conference on Isotope Geology (ACIG-16), Department of Geosciences and Natural Resource Management Faculty of Science University of Copenhagen Denmark, Proceeding Book; pp. 67-83.

**Shaltami, O.R., Fares, F.F., EL Oshebi, F.M., Errishi, H., Bustany, I., Salloum, F.M., El Shawaihdi, M.H. and Musa, M.M. (2018):** Absolute age of the Miocene deposits in the Cyrenaica Basin, NE Libya: Implications for the Messinian Salinity Crisis. IAEG Annual Conference 2018 - Geochemistry, Irish Association for Economic Geology; pp. 62-76.

**Shaltami, O.R., Fares, F.F., EL Oshebi, F.M., Errishi, H. and Santos, P. (2018):** New high-precision <sup>87</sup>Sr/<sup>86</sup>Sr ages on Late Oligocene-Early Miocene rocks in the Al Jabal Al Akhdar, NE Libya. International Conference on Advances in Chronostratigraphy (ICAC 2018), Bangkok, Thailand, Proceeding Book; pp. 57-66.

**Shaltami, O.R., Fares, F.F., EL Oshebi, F.M., Errishi, H. and Santos, P. (2018):** Paleoclimate across the Cretaceous/Paleogene boundary event: A case study of the Al Jabal Al Akhdar, NE Libya. Advanced Carbonate Geology, Kuala Lumpur, Malaysia, Proceeding Book; pp. 10-14.

**Shaltami, O.R., Fares, F.F., EL Oshebi, F.M., Errishi, H. and Santos, P. (2018):** Hydrology of the Mediterranean Sea during the Messinian Salinity Crisis: A case study of the Cyrenaica Basin, NE Libya. 64<sup>th</sup> Annual Institute on Lake Superior Geology, Iron Mountain, Michigan, USA, Proceeding Book; pp. 16-21.

**Shaltami, O.R., Fares, F.F., EL Oshebi, F.M., Errishi, H. and Souza, R. (2018):** Isotope geochronology of the Pliocene-Quaternary deposits in the Al Jabal Al Akhdar, NE Libya. International Conference on Applied Science and Engineering (ICASE), Bangkok, Thailand, Proceeding Book; pp. 21-29.

**Shaltami, O.R., Fares, F.F., Errishi, H., EL Oshebi, F.M. and Bustany, I. (2017):** Rare earth element geochemistry and isotope geochronology of the Quaternary calcarenites in the Al Jabal Al Akhdar, NE Libya. 10<sup>th</sup> International Conference on Applied Geochemistry (ICG-10), Institute of Geosciences Federal University of Rio Grande do Sul, Porto Alegre, Brazil, Proceeding Book; pp. 50-68.

**Shaltami, O.R., Fares, F.F., Errishi, H., EL Oshebi, F.M. and Bustany, I. (2018):** Redox conditions and depositional environment of the Tulmithah and Apollonia Formations, Al Jabal Al Akhdar, NE Libya. GeoBaikal 2018, Irkutsk, Russia, Proceeding Book; pp. 77-83.

**Shaltami, O.R., Fares, F.F., Errishi, H., EL Oshebi, F.M. and Souza, R. (2018):** Chemostratigraphy of the Al Abraaq Group, Cyrenaica Basin, NE Libya. 4<sup>th</sup> International Conference on Applied Science and Engineering (ICASE), Bhubaneswar, Odisha, Proceeding Book; pp. 30-39.

**Shaltami, O.R., Jorgensen, L., Elkjaer, C., Fares, F.F., Errishi, H., EL Oshebi, F.M. and Souza, R. (2018):** Petroleum geochemistry of the Qahash and Daryanah formations, Cyrenaica Basin, NE Libya. 4<sup>th</sup> Annual AAPG/EAGE/MGS Myanmar Oil & Gas Conference, Yangon, Myanmar, Proceeding Book; pp. 34-50.



**Shaltami, O.R., Liu, Y., Jorgensen, L., Elkjaer, C., Fares, F.F., Errishi, H., EL Oshebi, F.M. and Souza, R. (2019):** Chemostratigraphy of the Al Uwayliayah Formation, Cyrenaica Basin, NE Libya. International Conference on Geological and Environmental Sustainability (ICGES-19), Visakhapatnam India, Proceeding Book; pp. 49-57.

**Shaltami, O.R., Jorgensen, L., Elkjaer, C., Fares, F.F., Errishi, H., EL Oshebi, F.M. and Souza, R. (2019):** Gas geochemistry of reservoirs in the Cyrenaica Basin, NE Libya. International Conference on Geological and Environmental Engineering (ICGEE), New York, USA, Proceeding Book; pp. 13-23.

**Shaltami, O.R., Liu, Y., Jorgensen, L., Elkjaer, C., Fares, F.F., Errishi, H., EL Oshebi, F.M. and Souza, R. (2019):** Organic geochemistry of shale and marl: A case study of the Miocene deposits in the Cyrenaica Basin, NE Libya. World Chemistry 2019, Philadelphia, USA, Proceeding Book; pp. 70-82.

**Shaltami, O.R., Jorgensen, L., Elkjaer, C., Fares, F.F., Errishi, H., EL Oshebi, F.M. and Souza, R. (2019):** Petroleum Geochemistry of the Al Baniyah Formation, Cyrenaica Basin, NE Libya. 23th International Conference on Engineering, Technology and Applied Science (ETAS-23) Seoul, South Korea, Proceeding Book; pp. 13-21.

**Shaltami, O.R., Jorgensen, L., Elkjaer, C., Fares, F.F., Errishi, H., EL Oshebi, F.M. and Souza, R. (2019):** Petroleum geochemistry of the Al Bayda Group, Cyrenaica Basin, NE Libya. 12<sup>th</sup> International Conference on Applied Science and Engineering (ICASE), Bangkok, Thailand, Proceeding Book; pp. 43-57.

**Shaltami, O.R., Liu, Y., Jorgensen, L., Elkjaer, C., Fares, F.F., Errishi, H., EL Oshebi, F.M. and Souza, R. (2019):** Petroleum geochemistry of the Benghazi Formation, Cyrenaica Basin, NE Libya. 2019 SME Annual Conference & Expo, Denver, Colorado, USA, Proceeding Book; pp. 22-38.

**Shaltami, O.R., Liu, Y., Jorgensen, L., Elkjaer, C., Fares, F.F., Errishi, H., EL Oshebi, F.M. and Souza, R. (2019):** Petroleum Geochemistry of the Eocene Deposits, Cyrenaica Basin, NE Libya. 21st International Conference on Engineering, Technology and Applied Science (ETAS-21), Taipei, Taiwan, Proceeding Book; pp. 10-26.

**Shaltami, O.R., Liu, Y., Jorgensen, L., Elkjaer, C., Fares, F.F., Errishi, H., EL Oshebi, F.M. and Souza, R. (2019):** Petroleum Geochemistry of the Pliocene Deposits, Cyrenaica Basin, NE Libya. Petroleum Istanbul 2019, Turkey, Proceeding Book; pp. 11-29.

**Shanmugam, G. (1985):** Significance of coniferous rain forests and related organic matter in generating commercial quantities of oil, Gippsland Basin, Australia. American Association of Petroleum Geologists Bulletin; 69: 1241-1254.

**Silva, M.B., Kalkreuth, W. and Holz, M. (2008):** Coal petrology of coal seams from the Leão- Butiá Coalfield, Lower Permian of the Paraná Basin, Brazil- implications for coal facies interpretations. International Journal of Coal Geology; 73: 331-358.

**Singh, A., Shivanna, M., Mathews, R.P., Singh, B.D., Singh, H., Singh, V.P. and Dutta, S. (2017):** Paleoenvironment of Eocene lignite bearing succession from Bikaner- Nagaur Basin, western India: Organic petrography, palynology, palynofacies and geochemistry. International Journal of Coal Geology; 181: 87-102.

**Singh, V.K., Rajak, P.K. and Singh, P.K. (2019):** Revisiting the paleomires of western India: An insight into the early Paleogene lignite Corridor. Journal of Asian Earth Sciences; 171: 363-375.

**Stach, E. (1982):** Stach's text book of coal petrology, 3rd edition. Gebruder Borntraeger, Berlin/Stuttgart; 535p.

**Suarez-Ruiz, I., Flores, D., Mendonca Filho, J.G. and Hackley, P.C. (2012):** Review and update of the applications of organic petrology: Part 1, Geological applications. International Journal of Coal Geology; 22: 54-112.

**Swedan A. and Issawi, B. (1977):** Geological Map of Libya, 1:250,000, Sheet: Bir Hacheim, NI 34-4, Explanatory Booklet, Industrial Research Center (IRC), Tripoli, Libya, 80p.

**Sykes, R. and Snowdon, L.R. (2002):** Guidelines for assessing the petroleum potential of coaly source rocks using Rock-Eval pyrolysis. *Organic Geochemistry*; 33(12): 1441-1455.

**Taylor, G.H. and Cook, A.C. (1962):** Sclerotinite in coal-its petrology and classification. *Geological Magazine*; 99: 41-52.

**Taylor, G.H., Teichmuller, M., Davis, A., Diessel, C.F.K., Littke, R. and Robert, P. (1998):** *Organic Petrology*. Gebruder Borntraeger, Berlin; 704p.

**Tissot, B.P. and Welte, D.H. (1984):** *Petroleum formation and occurrence*, second edition. Springer Verlag, Berlin, 699p.

**Vandenbroucke, M. (2003):** Kerogen: from types to models of chemical structure. *Oil and Gas Science and Technology*; 58(2): 243-269.

**Vandenbroucke, M. and Largeau, C. (2007):** Kerogen origin, evolution and structure. *Organic Geochemistry*; 38(5); 719-833.

**Van Krevelen, D.W. (1961):** *Coal: typology-chemistry-physics-constitution*: Elsevier Science, Amsterdam; 514p.

**Van Krevelen, D.W. (1993):** *Coal*. 3rd Edition, Elsevier Science Publishers, Amsterdam.

**Wilkin, R. T. and Barnes, H. L. (1997):** Formation processes of framboidal pyrite. *Geochimica et Cosmochimica Acta*; 61(2): 323-339.

**Wust, R.A.J., Hawke, M.I. and Bustin, R.M. (2001):** Comparing maceral ratios from tropical peat lands with assumptions from coal studies: Do classic coal petrographic interpretation methods have to be discarded. *International Journal of Coal Geology*; 48: 115-132.

**Xia, L., Fenjin, S., Mingli, S., Zhihong, W., Fuying, Z., Zehui, Z., Li, X. and Feng, H. (2009):** Geochemistry of deep coal-type gas and gas source rocks in Songliao Basin. *Petroleum Exploration and Development*; 36(3): 339-346.

**Yandoka, B.M.S., Abdullah, W.H., Abubakar, M.B., Hakimi, M.H. and Adegoke, A.K. (2015):** Geochemical characterisation of Early Cretaceous lacustrine sediments of Bima Formation, Yola Sub-basin, Northern Benue Trough, NE Nigeria: Organic matter input, preservation, paleoenvironment and palaeoclimatic conditions. *Marine and Petroleum Geology*; 61: 82-94.

**Zert, B. (1974):** Geological map of Libya, 1:250000, Sheet: Darnah, NI 34-16, Explanatory Booklet, Industrial Research Center (IRC), Tripoli, 49p.

**Zhang, S., Tang, S., Tang, D., Pan, Z. and Yang, F. (2010):** The characteristics of coal reservoir pores and coal facies in Liulin district, Hedong coal field of China. *International Journal of Coal Geology*; 81: 117-127.

**Zhou, S. and Huang, H. (2008):** Controls on alkylphenol occurrence and distribution in oils from lacustrine rift basins in East China. *Science in China Series D: Earth Sciences*; 51(7): 976-983.

# الجيو كيمياء العضوية لتكوين قحاش في البئر البحري أ 1 - ن س 128 ، بحوض برقة شمال شرق ليبيا

قدمت من قبل :

عمر عادل عمر قنبر

تحت إشراف :

د. أسامة الشلطي

## الملخص

إن الغرض من هذه الأطروحة هو وصف محتوى المادة العضوية لصخرين مصدرين (الصخر الزيتي والفحم) حيث أنه تم جمعهما من تكوين القحاش في البئر البحري أ 1 - ن س 128 حوض برقة، شمال شرق ليبيا، وتتألف العينات التي تم دراستها بشكل رئيسي من فيترينايت ماساريل، تليها كمية معتدلة من اللبتينايت ماساريل وكمية منخفضة من الانرتايت ماساريل. مع ذلك فإن العينات تحتوي أيضا على كمية كبيرة من الفرمبويدال بايرايت. تشير مؤشرات (VI، GWI، GI، TPI) إلى حالة ليمنوتيلماتيك أثناء ترسب الصخور الزيتيه والفحم. من الناحية الجيوكيميائية، يتمتع تكوين قحاش الطين الصفائحي بنوعية جيدة من المادة العضوية، في حين أن الفحم الحجري يعتبر صخرة مصدر فقير. من ناحية اخرى، يحتوي تكوين قحاش الطين الصفائحي على الكيروجين من النوع 2 / 3 (المادة العضوية المختلطة)، في حين أن فحم القحاش يحتوي على النوع 3 و 4 من (المادة العضوية). المادة العضوية غير ناضجة حراريا. تم ترسيب القحاش في بيئة عالية الملوحة.

الكلمات الدالة:

الصخور العضوية ، الجيوكيمياء العضوية ، صخور المصدر ، تكوين قحاش ، حوض برقة ، ليبيا.



**الجيوكيمياء العضوية لتكوين قحاش في البئر البحري  
أ 1 - ن س 128 ، بحوض برقة ، شمال شرق ليبيا  
قدمت من قبل :**

**عمر عادل عمر قنبر**

**تحت إشراف :**

**د. أسامة الشلطي**

**قدمت هذه الرسالة استكمالاً لمتطلبات الحصول على درجة الماجستير في علم**

**الجيوكيمياء**

**جامعة بنغازي**

**كلية العلوم**

**ديسمبر 2019**